Förster Resonance Energy Transfer
FRET

I should note before we start that the Merriam-Webster online dictionary defines “FRET” as:

“to cause to suffer emotional strain”

This sentence appears in a 2006 book!
Let's correct this mistake!

More than 50 years ago, the German scientist Förster discovered that close proximity of two chromophores changes their spectral properties in predictable ways (Förster, 1948a).

Milestones in the Theory of Resonance Energy Transfer

1922 G. Cario and J. Franck demonstrate that excitation of a mixture of mercury and thallium atomic vapors with 254nm (the mercury resonance line) also displayed thallium (sensitized) emission at 535nm.

1924 E. Gaviola and P. Pringsham observed that an increase in the concentration of fluorescein in viscous solvent was accompanied by a progressive depolarization of the emission.

1925 J. Perrin proposed the mechanism of resonance energy transfer

1928 H. Kallmann and F. London developed the quantum theory of resonance energy transfer between various atoms in the gas phase. The dipole-dipole interaction and the parameter R_0 are used for the first time

1932 F. Perrin published a quantum mechanical theory of energy transfer between molecules of the same specie in solution. Qualitative discussion of the effect of the spectral overlap between the emission spectrum of the donor and the absorption spectrum of the acceptor

1946-1949 T. Förster develop the first complete quantitative theory of molecular resonance energy transfer

What is FRET ?

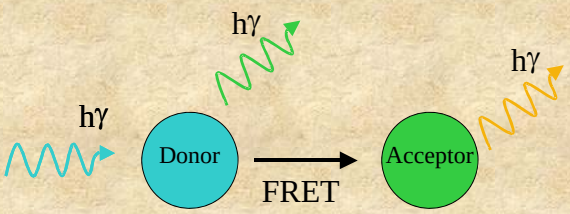

When the donor molecule absorbs a photon, and there is an acceptor molecule close to the donor molecule, radiationless energy transfer can occur from the donor to the acceptor.

FRET results in a decrease of the fluorescence intensity and lifetime of the donor probe, It enhance the fluorescence of the acceptor probe when the acceptor is fluorescent.

PM

Tuning fork analogy for resonance energy transfer

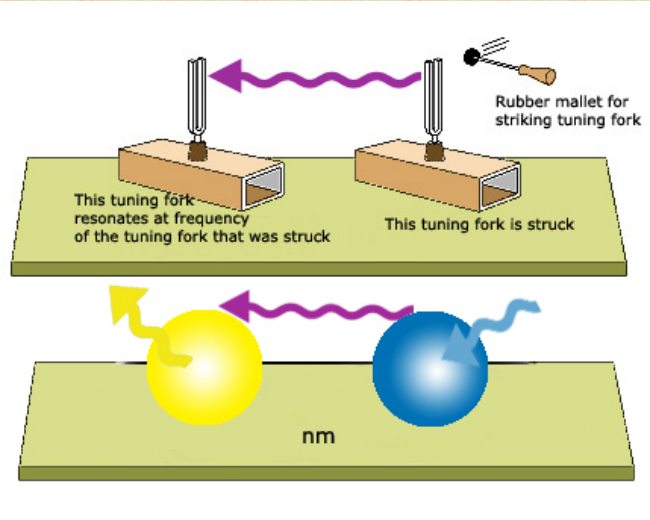

TV

Simplified FRET Energy Diagram

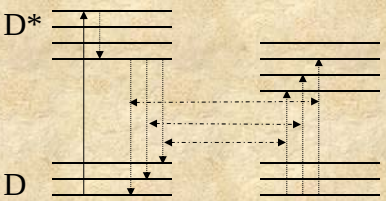

Coupled transitions

Suppose that the energy difference for one of these possible deactivation processes in the donor molecule matches that for a possible absorption transition in a nearby acceptor molecule. Then, with sufficient energetic coupling between these molecules (overlap of the emission spectrum of the donor and absorption spectrum of the acceptor), both processes may occur simultaneously, resulting in a transfer of excitation from the donor to the acceptor molecule

The interaction energy is of a dipole-dipole nature and depends on the distance between the molecules as well as the relative orientation of the dipoles

PM

Dipole-dipole interaction

The rate of transfer (k_T) of excitation energy is given by:

$$k_T = (1/\tau_d)(R_0/r)^6$$

Where τ_d is the fluorescence lifetime of the donor in the absence of acceptor, r the distance between the centers of the donor and acceptor molecules and R_0 the Förster critical distance at which 50% of the excitation energy is transferred to the acceptor and can be approximated from experiments independent of energy transfer.

Förster critical distance

$$R_0 = 0.2108\,(n^{-4} Q_d \kappa^2 J)^{1/6} \text{ Å}$$

n is the refractive index of the medium in the wavelength range where spectral overlap is significant (usually between 1.2-1.4 for biological samples)

Q_d is the fluorescence quantum yield of the donor in absence of acceptor (i.e. number of quanta emitted / number of quanta absorbed)

κ^2 (pronounced "kappa squared") is the orientation factor for the dipole-dipole interaction

J is the normalized spectral overlap integral [$\varepsilon(\lambda)$ is in $M^{-1}\,cm^{-1}$, λ is in nm and J units are $M^{-1}\,cm^{-1}\,(nm)^4$]

The overlap integral *J* is defined by:

$$J = \int_0^\infty I_D(\lambda)\varepsilon_A(\lambda)\lambda^4 d\lambda$$

Where λ is the wavelength of the light, $\varepsilon_A(\lambda)$ is the molar absorption coefficient at that wavelength and $I_D(\lambda)$ is the fluorescence spectrum of the donor normalized on the wavelength scale:

$$I_D(\lambda) = \frac{F_{D\lambda}(\lambda)}{\int_0^\infty F_{D\lambda}(\lambda)d\lambda}$$

Where $F_{D\lambda}(\lambda)$ is the donor fluorescence per unit wavelength interval

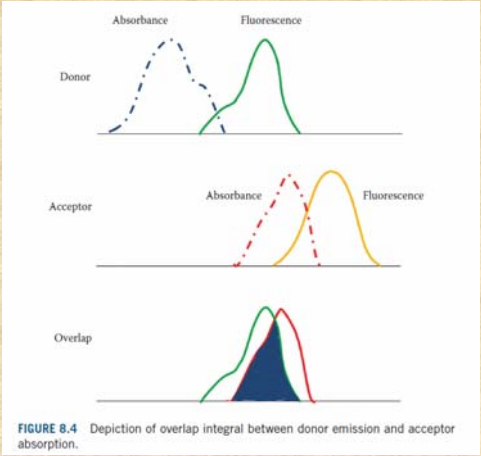

FIGURE 8.4 Depiction of overlap integral between donor emission and acceptor absorption.

Determination of the efficiency of energy transfer (*E*)

Steady state method: *Decrease in donor fluorescence.* the fluorescence intensity of the donor is determined in absence and presence of the acceptor.

$$E = 1 - \frac{F_{da}}{F_d}$$

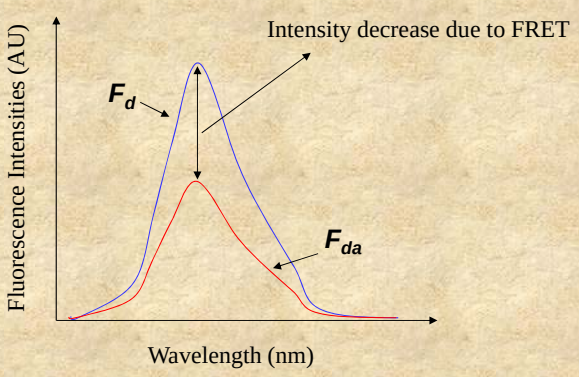

Determination of the efficiency of energy transfer (*E*)

Time-resolved method: Decrease in the lifetime of the donor

If the fluorescence decay of the donor is a single exponential then:

$$\mathbf{E = 1 - \frac{\tau_D}{\tau_D^0}}$$

Where τ_D and τ_D^0 are the lifetime of the donor in the presence and absence of acceptor, respectively

Determination of the efficiency of energy transfer (*E*)

If the donor fluorescence decay in absence of acceptor is not a single exponential (probably resulting from heterogeneity of the probe's microenvironment) , then it may be modeled as a sum of exponential and the transfer efficiency can be calculated using the average decay times of the donor in absence and presence of acceptor:

$$E = 1 - \frac{\langle \tau_D \rangle}{\langle \tau_D^0 \rangle}$$

Where $\langle\tau\rangle$ is the amplitude-average decay time and is defined as:

$$\langle \tau \rangle = \frac{\sum_i \alpha_i \tau_i}{\sum_i \alpha_i}$$

The distance dependence of the energy transfer efficiency (*E*)

$$r = \left(\frac{1}{E} - 1\right)^{1/6} R_0$$

Where *r* is the distance separating the donor and acceptor fluorophores, R_0 is the Förster distance.

Many equivalent forms of this equation is found in the literature, such as:

$$E = R_0^6 / (R_0^6 + r^6) \text{ or } E = 1 / \left[1 + \left(r/R_0\right)^6\right]$$

The distance dependence of the energy transfer efficiency (*E*)

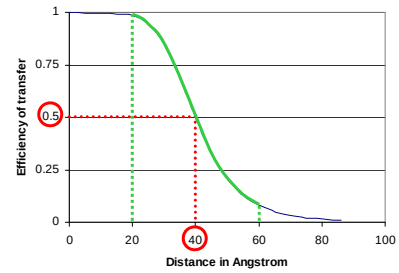

The efficiency of transfer varies with the inverse sixth power of the distance.

R_0 in this example was set to 40 Å. When the *E* is 50%, $R=R_0$

Distances can usually be measured between 0.5 R_0 and ~1.5R_0. Beyond these limits, we can often only say that the distance is smaller than 0.5 R_0 or greater than 1.5R_0. If accurate distance measurement is required then a probe pair with a different R_0 is necessary.

How was FRET theory tested experimentally?

Energy Transfer. A System with Relatively Fixed Donor–Acceptor Separation

JACS 87:995(1965)

S. A. Latt, H. T. Cheung, and E. R. Blout

Contribution from the Department of Biological Chemistry, Harvard Medical School, Boston, Massachusetts. *Received August 24, 1964*

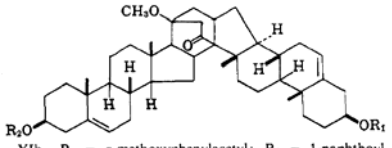

XIb, R_1 = *p*-methoxyphenylacetyl; R_2 = 1-naphthoyl
XIIb, R_1 = 1-naphthoyl; R_2 = anthracene-9-carbonyl

Table III

Compound	$\overline{K^2}$	R_{calcd}, Å.	R_{meas} (from Dreiding models), Å.
XI	$^2/_3$	21.3 ± 1.6	21.8 ± 2.0 (linear av.) 19.2 ± 2.0 ($[\overline{1/R^6}]^{-1/6}$)
XII	$^2/_3$	16.7 ± 1.4	21.5 ± 2.0 (linear av.) 19.4 ± 2.0 ($[\overline{1/R^6}]^{-1/6}$)

The most likely explanation for this discrepancy between the predicted and observed transfer in compound XII is that the value of the average orientation factor is greater than the estimate of $^2/_3$ which was used to calculate the predicted separation.

*DEPENDENCE OF THE KINETICS OF SINGLET-SINGLET ENERGY TRANSFER ON SPECTRAL OVERLAP**

BY RICHARD P. HAUGLAND,† JUAN YGUERABIDE,‡ AND LUBERT STRYER‡

DEPARTMENT OF CHEMISTRY, STANFORD UNIVERSITY, AND
DEPARTMENT OF BIOCHEMISTRY, STANFORD UNIVERSITY SCHOOL OF MEDICINE

Communicated by Harden M. McConnell, February 19, 1969

PNAS

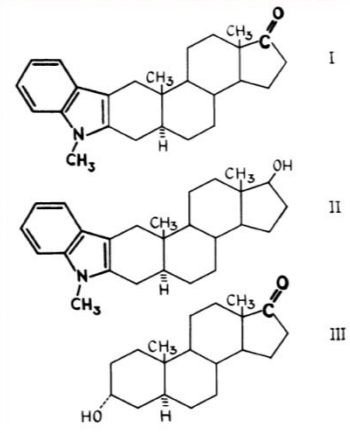

I II III

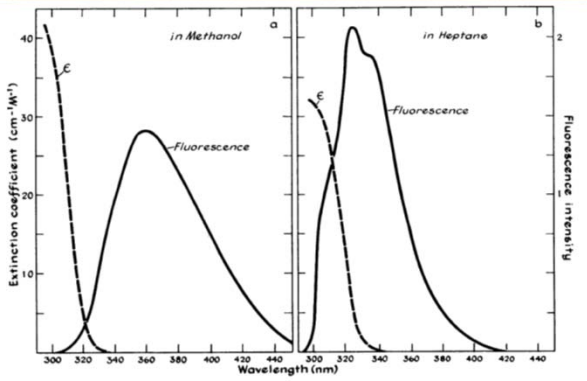

FIG. 2.—Overlap of the emission spectrum of the N-methylindole energy donor (II) and the absorption spectrum of the ketone energy acceptor (III) in (*a*) methanol and (*b*) heptane. III is nonfluorescent.

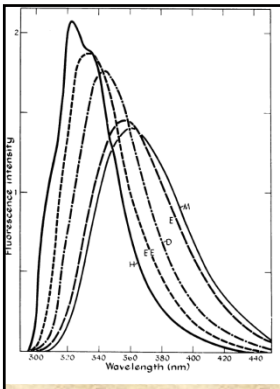

FIG. 3.—Fluorescence emission spectra of II in n-heptane (*H*), ethyl ether (*EE*), p-dioxane (*D*), ethanol (*E*), and methanol (*M*). The spectrum of II in ethyl acetate is virtually identical to that obtained in dioxane. The intensities have been normalized so that the areas under the curves are equal. The excitation wavelength was 290 nm.

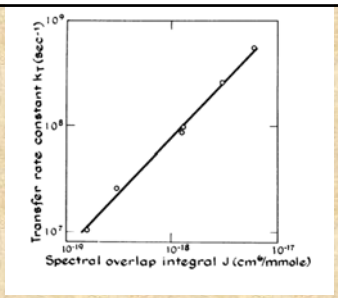

TABLE I. *Fluorescence properties of I and II in a series of solvents.*

Solvent	τ_I (nsec)	τ_{II} (nsec)	Fluorescence Quantum Yield Q_I	Q_{II}	Transfer Efficiency E_K	E_{SS}
Methanol	5.3	5.6	0.397	0.420	0.053	0.055
Ethanol	5.6	6.5	0.440	0.510	0.14	0.138
Dioxane	3.6	5.4	0.360	0.535	0.33	0.328
Ethyl acetate	3.3	4.7	0.286	0.418	0.30	0.315
Ethyl ether	2.1	4.5	0.247	0.515	0.53	0.52
Heptane	1.1	2.8	0.136	0.346	0.606	0.608

TABLE 2. *Transfer kinetics and spectral overlap integral of I in a series of solvents.*

Solvent	Transfer rate, k_T(sec^{-1}) $\times 10^{-7}$	Spectral overlap integral, J(cm^6 mmole^{-1}) $\times 10^{19}$	k_F (sec^{-1}) $\times 10^{-7}$	n_D	k_T/J $\times 10^{-26}$	$k_T/(Jk_F)$ $\times 10^{-18}$
Methanol	1.0	1.5	7.50	1.331	0.67	0.89
Ethanol	2.5	3.0	7.85	1.362	0.83	1.06
Dioxane	9.6	13.0	9.9	1.423	0.74	0.75
Ethyl acetate	11.3	12.8	8.9	1.372	0.88	0.99
Ethyl ether	25.5	30.0	11.5	1.349	0.83	0.72
Heptane	55.2	60.3	12.4	1.387	0.92	0.74

r^{-6} distance dependence?

$$k_T = (1/\tau_d)(R_0/r)^6$$

*ENERGY TRANSFER: A SPECTROSCOPIC RULER**

BY LUBERT STRYER AND RICHARD P. HAUGLAND†

DEPARTMENT OF BIOCHEMISTRY, STANFORD UNIVERSITY SCHOOL OF MEDICINE, PALO ALTO, AND THE DEPARTMENT OF CHEMISTRY, STANFORD UNIVERSITY

Communicated by Arthur Kornberg, May 29, 1967 PNAS

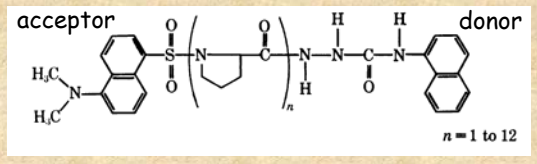

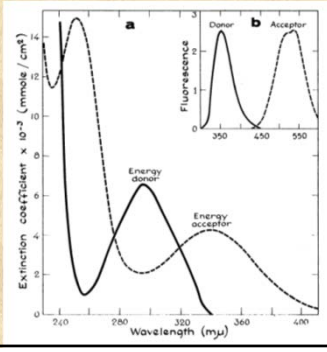

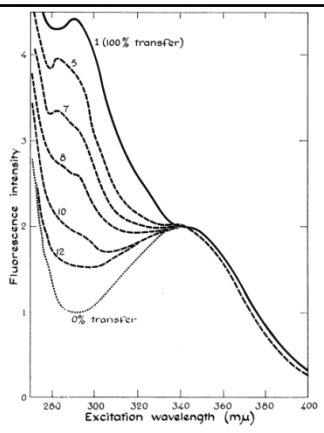

FIG. 3.—Excitation spectrum of dansyl-L-prolyl-hydrazide (· · · · ·, 0% transfer), dansyl-L-prolyl-α-naphthyl (———, 100% transfer), and dansyl-(L-prolyl)$_n$-α-naphthyl (– – – –, n = 5, 7, 8, 10, 12) in ethanol.

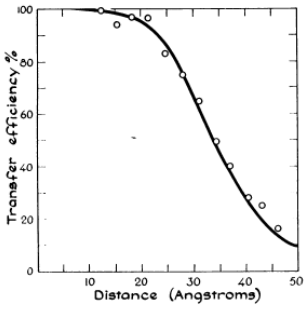

FIG. 4.—Efficiency of energy transfer as a function of distance in dansyl-(L-prolyl)$_n$-α-naphthyl, n = 1 to 12. The α-naphthyl and dansyl groups were separated by defined distances ranging from 12 to 46 Å. The energy transfer is 50% efficient at 34.6 Å. The solid line corresponds to an r^{-6} distance dependence.

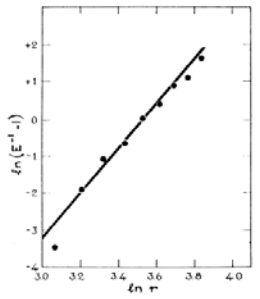

FIG. 5.—The dependence of the efficiency of energy transfer on distance is given by the slope in this plot of ln $(E^{-1} - 1)$ versus ln r. The slope is 5.9, in excellent agreement with the r^{-6} dependence predicted by Förster.

For these parameters, R_0 is calculated to be 27.2 Å, while the observed value is 34.6 Å (Figs. 4 and 5). A rigorous comparison of the observed and calculated R_0 distances should be deferred until the value of K^2 is better defined. It would also be desirable to have independent confirmation of the estimated distances between the energy donor and acceptor groups.

More to the story???

Effect of flexibility and *cis* residues in single-molecule FRET studies of polyproline

Robert B. Best*†, Kusai A. Merchant*, Irina V. Gopich*, Benjamin Schuler*‡, Ad Bax*, and William A. Eaton*§

18964–18969 | PNAS | November 27, 2007 | vol. 104 | no. 48

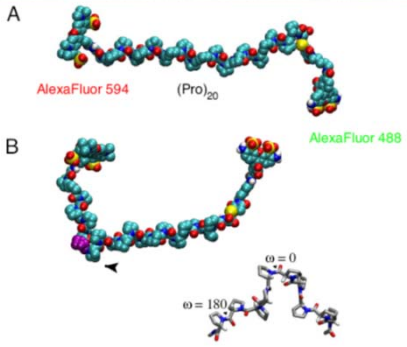

Fig. 1. Polyproline structures. Space-filling representation of polyproline-20 labeled with Alexa Fluor 488 (FRET donor) at the C-terminal cysteine and Alexa Fluor 594 (FRET acceptor) at the N-terminal glycine in the *all-trans* conformation (*A*) and with residue 8 (purple) in the *cis* conformation (*B*). (*B Inset*) A polyproline fragment with one *cis* peptide bond (shown as "ω = 0"). One of the remaining *trans* peptide bonds is also indicated ("ω = 180").

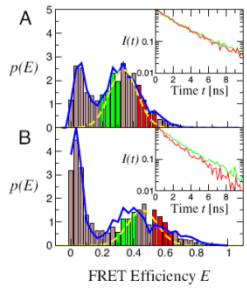

Fig. 3. Distributions of FRET efficiency for polyproline-20. The efficiency of each molecule $E = n_A/(n_A + n_D)$ was calculated from the (γ-corrected) n_A acceptor and n_D donor photons detected as it passes through the observation volume, in TFE (*A*) and water (*B*) (solid bars). Broken yellow lines indicate the shot-noise-limited width of the distribution (24, 19). Solid blue line in *A* gives a maximum likelihood fit of the data a multistate model. Solid blue line in *B* gives the expected efficiency distribution for a heterogeneous mixture of species containing *cis* proline, taking the relative populations from NMR and the efficiencies from simulation. (*Insets*) The donor fluorescence decays for donor photons from the subpopulations with corresponding colors in the efficiency histograms.

Distributions

Proc. Nat. Acad. Sci. USA
Vol. 68, No. 9, pp. 2099–2101, September 1971

Determination of Distance Distribution Functions by Singlet-Singlet Energy Transfer

(flexibility/Förster theory/fluorescence/molecular structure)

CHARLES R. CANTOR AND PHILIP PECHUKAS

Proc. Nat. Acad. Sci. USA
Vol. 69, No. 8, pp. 2273–2277, August 1972

Evaluation of the Distribution of Distances Between Energy Donors and Acceptors by Fluorescence Decay

(energy transfer/fluorescence/decay/conformation/polymers)

A. GRINVALD, E. HAAS, AND I. Z. STEINBERG

$$E(R_0) = \int_0^\infty dR\, f(R)\, \frac{R_0^6}{R_0^6 + R^6}$$

Distributions

Proc. Nat. Acad. Sci. USA
Vol. 72, No. 5, pp. 1807–1811, May 1975

Distribution of End-to-End Distances of Oligopeptides in Solution as Estimated by Energy Transfer

(fluorescence decay/conformation)

ELISHA HAAS, MEIR WILCHEK, EPHRAIM KATCHALSKI-KATZIR, AND IZCHAK Z. STEINBERG

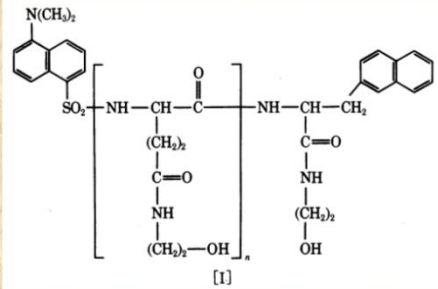

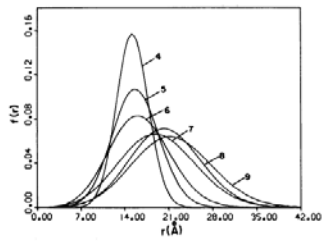

FIG. 4. The distribution function of the distances between donor and acceptor for the series of oligopeptides I, n = 4, 5, 6, 7, 8, and 9. The numbers in the figure refer to the values of n.

Distributions

Biochemistry **1988**, *27*, 9149–9160 9149

Distance Distributions in Proteins Recovered by Using Frequency-Domain Fluorometry. Applications to Troponin I and Its Complex with Troponin C†

Joseph R. Lakowicz,*,‡ Ignacy Gryczynski,‡,§ Herbert C. Cheung,∥ Chien-Kao Wang,∥ Michael L. Johnson,⊥ and Nanda Joshi‡

5238 *Biochemistry* **1991**, *30*, 5238–5247

Distance Distributions and Anisotropy Decays of Troponin C and Its Complex with Troponin I†

Herbert C. Cheung,*,‡ Chien-Kao Wang,‡§ Ignacy Gryczynski,‡ Wieslaw Wiczk,‡ Gabor Laczko,‡ Michael L. Johnson,⊥ and Joseph R. Lakowicz‡

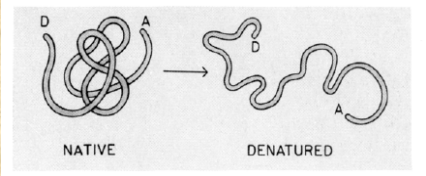

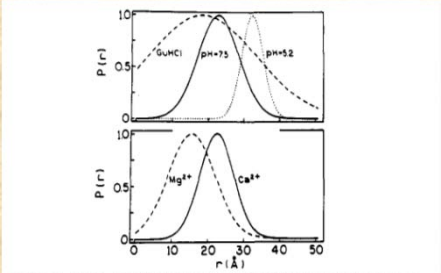

FIGURE 4: Distance distributions for TnC–DNZ–IAE in the absence of cations (top) and in the presence of Mg^{2+} and Ca^{2+} (pH 7.5, bottom). The pH for guanidine hydrochloride (GuHCl) was 7.5.

The orientation factor κ^2

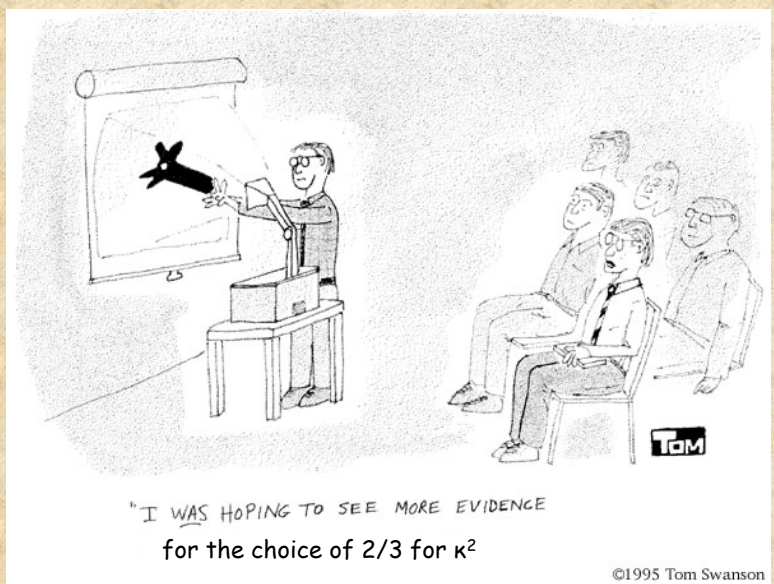

"I WAS HOPING TO SEE MORE EVIDENCE

for the choice of 2/3 for κ^2

The orientation factor κ^2

$$\kappa^2 = (\cos\theta_T - 3\cos\theta_D \cos\theta_A)^2$$

Where θ_T is the angle between the D and A moments, given by

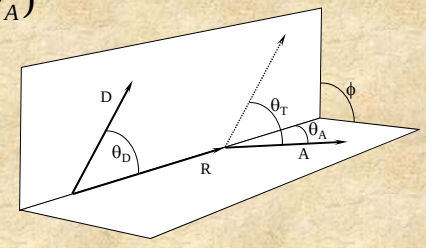

$$\cos\theta_T = \sin\theta_D \sin\theta_A \cos\phi + \cos\theta_D \cos\theta_A$$

In which θ_D, θ_A are the angles between the separation vector R, and the D and A moment, respectively, and ϕ is the azimuth between the planes (D,R) and (A,R)

The orientation factor κ^2

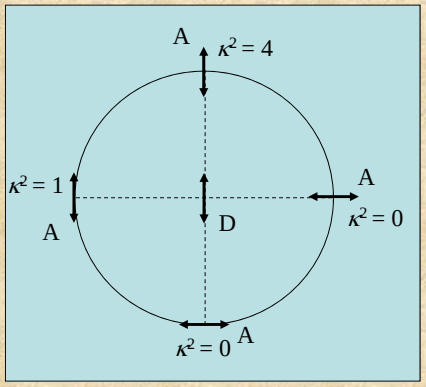

The limits for κ^2 are 0 to 4, The value of 4 is only obtained when both transitions moments are in line with the vector R. The value of 0 can be achieved in many different ways.

If the molecules undergo fast isotropic motions (dynamic averaging) then $\kappa^2 = 2/3$

From Eisinger and Dale in:"Excited States of Biological Molecules" Edited by John Birks (1976)

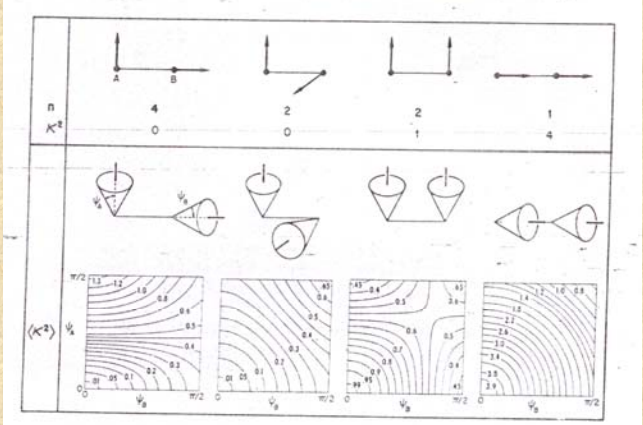

Figure 1 The upper part of the diagram illustrates the nine possible relative orientations of two transition dipoles each of which is fixed and can lie along either the x, y or z axis of a Cartesian triad. The corresponding κ^2 values are shown along with their statistical weights (n) and they are seen to lead to an average for κ^2 of 2/3, the same as for isotropically random orientations of the transition dipole moments. The lower part of the figure illustrates how these $\langle\kappa^2\rangle$ values change as the transition dipole directions are permitted orientational freedom within cones of half-angles ψ_A and ψ_B. Note that $\langle\kappa^2\rangle$ departs quite slowly from its fixed minimum and maximum values (0 and 4) as the two cones open up and that when each cone half-angle is $\pi/2$, corresponding to an isotropic distribution of the transition dipole directions, $\langle\kappa^2\rangle$ is equal to 2/3 for each of the cases considered

What if the system is static but randomly oriented?

For example for a system in a highly viscous solvent or in general if the fluorescence lifetimes are very short relative to any rotational motion.

Then $\kappa^2 = 0.476$

THE JOURNAL OF CHEMICAL PHYSICS VOLUME 48, NUMBER 6 15 MARCH 1968

Nonradiative Energy Transfer in Systems in which Rotatory Brownian Motion is Frozen

IZCHAK Z. STEINBERG

The Weizmann Institute of Science, Rehovoth, Israel

(Received 28 August 1967)

The effect of the complete restriction of rotatory Brownian motion of donor and acceptor molecules on the extent of nonradiative energy transfer in systems containing many donors and acceptors has been investigated. It is assumed that the molecules under discussion are randomly distributed and randomly oriented in space at the moment of excitation. The number of donor molecules which retain their excitation energy at time t after excitation is found to decrease exponentially with the sum of two terms: one proportional to t and the other proportional to $t^{1/3}$. This time dependence is similar in form to that found by Förster for systems in which donor and acceptor molecules undergo rapid rotatory diffusion. While the coefficient of $-t$ in the exponent is the same in both cases, the coefficient of $-t^{1/3}$ is smaller for systems in which molecular rotation is frozen than for systems in which rotatory Brownian motion is rapid.

This scenario may be very relevant to those wishing to do FRET on Fluorescent Proteins in cells
Why? Because the lifetimes are very short relative to any rotational motion

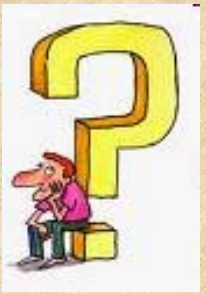

So how do we determine κ^2?

Except in very rare cases, κ^2 can not be uniquely determined in solution.

What value of κ^2 should be used ?

We can **assume** fast isotropic motions of the probes and the value of $\kappa^2 = 2/3$.

We can **calculate** the lower and upper limit of κ^2 using polarization spectroscopy (Dale, Eisinger and Blumberg 1979).

Lower and upper limit of κ^2

We can **calculate** the lower and upper limit of κ^2 using polarization (Dale, Eisinger and Blumberg 1979).

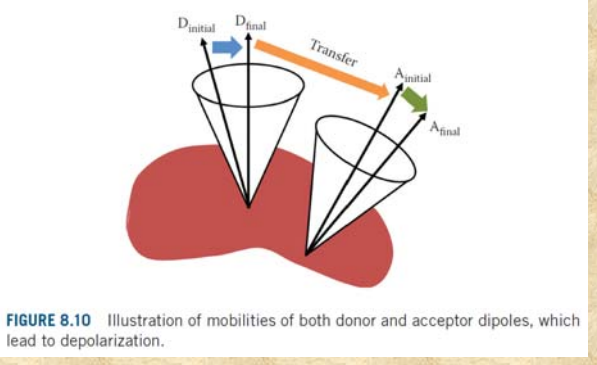

FIGURE 8.10 Illustration of mobilities of both donor and acceptor dipoles, which lead to depolarization.

Lets consider that each probe is rotating within a cone of axes D and A for the donor and acceptor, respectively, then 3 depolarization steps occur after the absorption of the excitation energy by the donor: An axial depolarization of the donor, a depolarization due to transfer and an axial depolarization of the acceptor

In the Dale-Eisinger-Blumberg approach, one measures the ratio of the observed polarizations of donors and acceptors to their limiting polarizations and then uses the calculated contour plots to put limits on κ^2

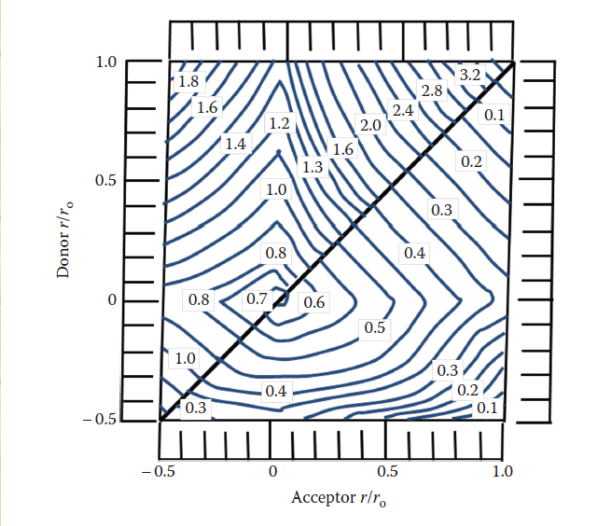

This approach was used in:
Arbildua et al.,
Fluorescence resonance energy transfer and molecular modeling studies on 4',6-diamidino-2-phenylindole (DAPI) complexes with tubulin.
Protein Sci. (2006) 15(3):410-9.

FRET occurs between DAPI and TNP-GTP bound to tubulin – a heterodimer protein

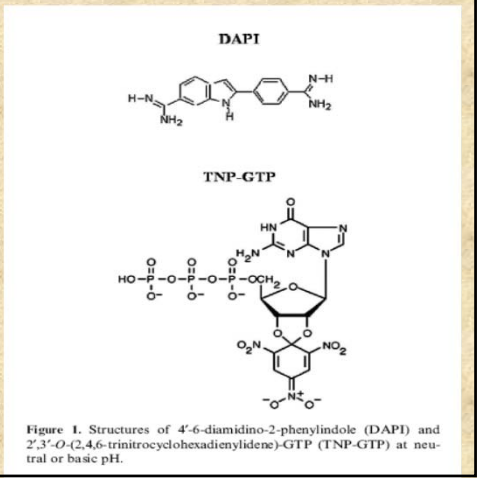

Figure 1. Structures of 4′-6-diamidino-2-phenylindole (DAPI) and 2′,3′-*O*-(2,4,6-trinitrocyclohexadienylidene)-GTP (TNP-GTP) at neutral or basic pH.

Assuming a κ^2 value of 2/3, one would calculate the DAPI-TNP-GTP distance to be ~43 Angstoms

But DAPI is bound non-covalently - hence has no local motion so its polarization is high (~0.42)

And, TNP-GTP is also non-covalently bound and has a short lifetime and hence a high polarization (~0.48)

These observed polarization values are close to the limiting polarization values for these probes: 93% and 100% respectively, for DAPI and TNP-GTP

Using the Dale-Eisenger-Blumberg plot one can then estimate that κ^2 can be anywhere between 0.02 and 3.7!

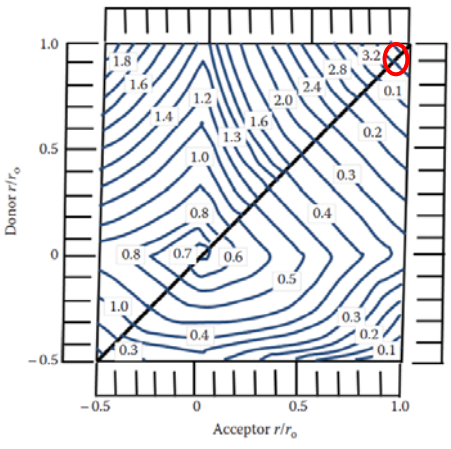

In fact the authors concluded, based on other information, that the distance between DAPI and TNP-GTP bound to tubulin was likely to ~ 30 Angstroms.

Quantitative distance determinations using FRET – i.e., as a true “spectroscopic ruler” - remain **difficult at best**

But FRET can be very powerful when used to detect changes in a system, such as alterations in distance and or orientation between donor and acceptor attached to biomolecules, i.e., due to ligand binding or protein-protein interactions

The renaissance of fluorescence resonance energy transfer

Paul R. Selvin

Recent advances in fluorescence resonance energy transfer have led to qualitative and quantitative improvements in the technique, including increased spatial resolution, distance range, and sensitivity. These advances, due largely to new fluorescent dyes, but also to new optical methods and instrumentation, have opened up new biological applications.

nature structural biology • volume 7 number 9 • september 2000

The development of Fluorescent Proteins has led to a significant increase in FRET studies

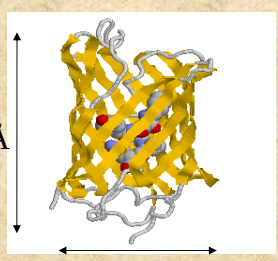

Fluorescent proteins with the appropriate absorption and emission properties are chosen as donors and acceptors. Such systems can be used in vitro as well as in vivo

The GFP is fused to the protein of interest and expressed in the organism under study.

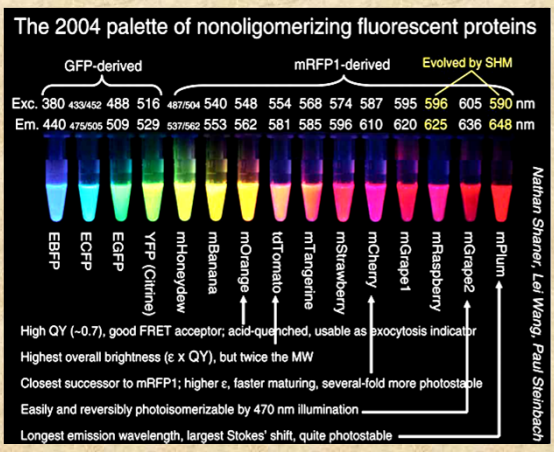

Homo-transfer of electronic excitation energy

So far, we considered the donor and acceptor molecules to be different. However, if the probe excitation spectrum overlaps its emission spectrum, FRET can occur between identical molecules.

« Il suffit qu'un transfert d'activation puisse se produire entre deux molécules voisines d'orientation différentes, c'est a dire portant des oscillateurs non parallèles, pour qu'il en résulte en moyenne une diminution de l'anisotropie de distribution des oscillateurs excites et par suite de la polarisation de la lumière émise. »

(F. Perrin *Ann de Phys.* 1929)

It suffices that a transfer of activation can occur between two neighboring molecules with different orientations, that is with non-parallel oscillators, in order to have, on average, a decrease in the anisotropy of the distribution of excited oscillators, and therefore a decrease of the polarization of the emitted light.

« …L'existence de transferts d'activation est expérimentalement prouvée pour de telles molécules par la décroissance de la polarisation de la lumière de fluorescence quand la concentration croit… »
(F. Perrin *Ann de Phys.* 1932)

…The existence of transfer of activation is proven experimentally for such molecules by the decrease in polarization of the fluorescent light when the concentration is increased…

Electronic energy transfer between identical fluorophores was originally observed by Gaviola and Pringsheim in 1924.

Über den Einfluß der Konzentration auf die Polarisation der Fluoreszenz von Farbstofflösungen.

Von **E. Gaviola** und **Peter Pringsheim** in Berlin.

Mit zwei Abbildungen. (Eingegangen am 24. März 1924.)

Tabelle 2. Uranin in ganz wasserfreiem Glycerin.

C	p	C	p	C	p	C	p
$\frac{1}{4}$	0	$\frac{1}{32}$	6,5	$\frac{1}{256}$	15	$\frac{1}{2048}$	39,2
$\frac{1}{8}$	?	$\frac{1}{64}$	8,1	$\frac{1}{512}$	19,5	$\frac{1}{4100}$	43,5
$\frac{1}{16}$	3,2	$\frac{1}{128}$	11,1	$\frac{1}{1024}$	30,7	etwa $\frac{1}{20000}$	45

(note: uranin is the sodium salt of fluorescein)

Homo-transfer of electronic excitation energy

"…Excitation transfer between alike molecules can occur in repeated steps. So the excitation may *migrate* from the absorbing molecule over a considerable number of other ones before deactivation occurs by fluorescence or other process. Though this kind of transfer cannot be recognized from fluorescence spectra, it may be observed by the decrease of fluorescence polarization…" (Förster, 1959)

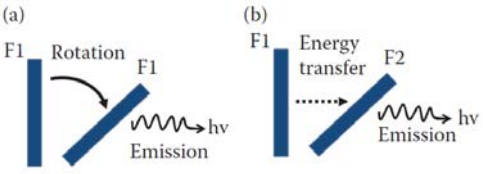

FIGURE 5.29 Depiction of depolarization due to (a) rotational diffusion and (b) energy transfer.

A. Depolarization resulting from rotational diffusion of the fluorophore. The excited fluorophore (F1*) rotates then emits light. **B.** The excited fluorophore (F1*) transfer energy to another fluorophore F2 which in turn emits light.

Weber's Red-Edge Effect

In 1960 Weber was the first to report that homotransfer among indole molecules disappeared upon excitation at the red-edge of the absorption band - this phenomenon is now known as the "Weber red-edge effect".

In 1970 Weber and Shinitzky published a more detailed examination of this phenomenon. They reported that in the many aromatic residues examined, transfer is much decreased or undetectable on excitation at the red edge of the absorption spectrum .

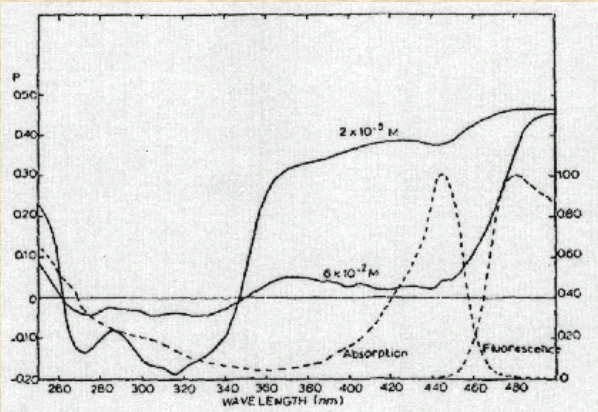

Distance determination using homotransfer

The efficiency of transfer can be calculated from a knowledge of the polarization in the absence and presence of energy transfer.

The steady state expression for the efficiency of energy transfer (*E*) as a function of the anisotropy is given by

$$E = 2(r_d - \langle r \rangle)/(r_d - r_a)$$

Where r_d and r_a are the anisotropy decay of the donor and acceptor only, respectively and $\langle r \rangle$ is the observed anisotropy in presence of both donor and acceptor. If κ^2 =2/3 then r_a = 0 and

$$E = 2(r_d - \langle r \rangle)/r_d$$

An example of homo-FRET used to study protein interactions is the work by Hamman et al (Biochemistry *35*:16680) on a prokaryotic ribosomal protein

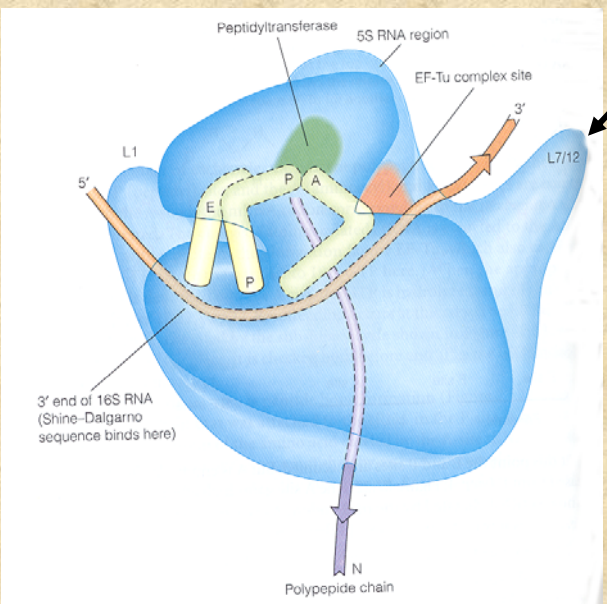

L7/L12 is present as two dimers in the ribosome. An X-ray structure of monomeric C-terminal domains led to the speculation that the C-terminal domains of L7/L12 interacted through hydrophobic surfaces as shown below

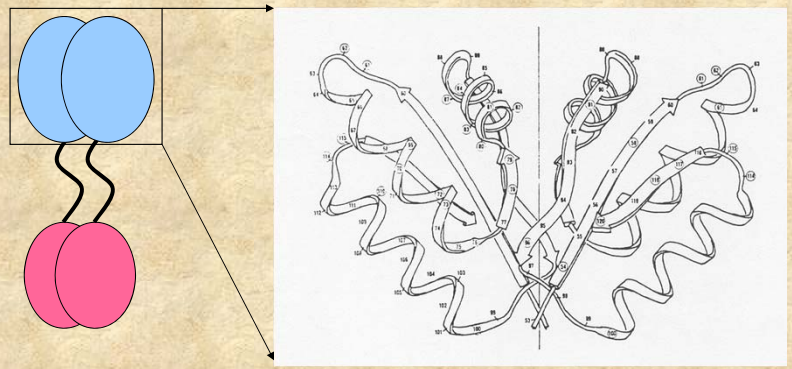

To study this protein fluorescence probes were introduced at specific locations along the L7/L12 peptide backbone.

To introduce these probes at specific locations site-directed mutagenesis was used to place cysteine residues in different locations

Sulfhydryl-reactive fluorescence probes were then covalently attached to these cysteine residues

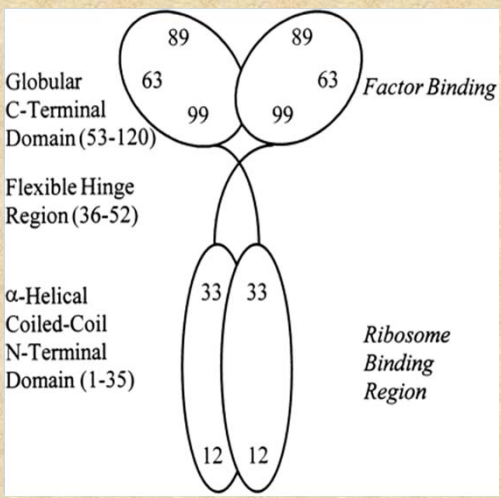

Subunit exchange experiments allowed the preparation of singly labeled dimers

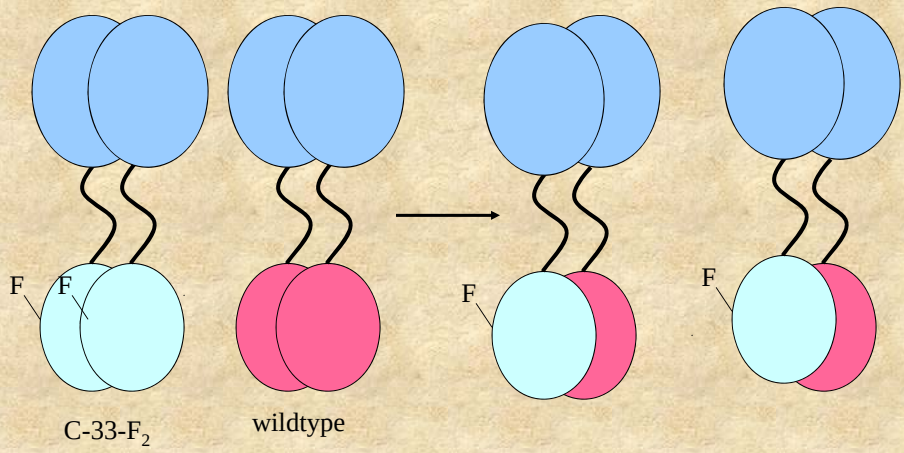

The presence of homoFRET was evident in the excitation polarization spectrum as shown by the Weber Red-Edge Effect.

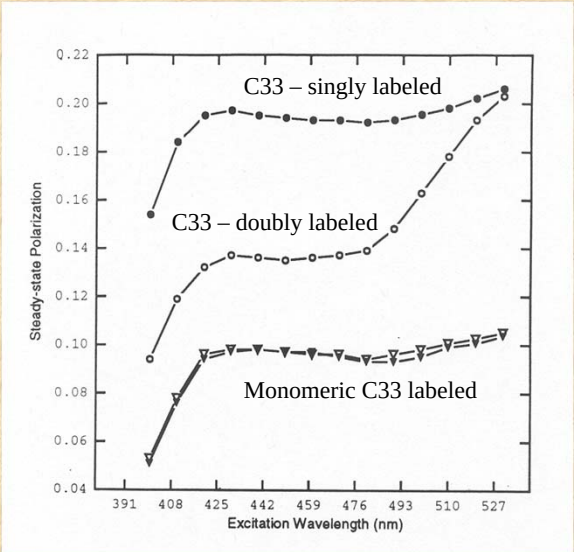

The polarization values, before and after subunit exchange, indicate which residues undergo homoFRET. The polarization data below are for fluorescein labeled constructs before (violet) and after (magenta) subunit exchange

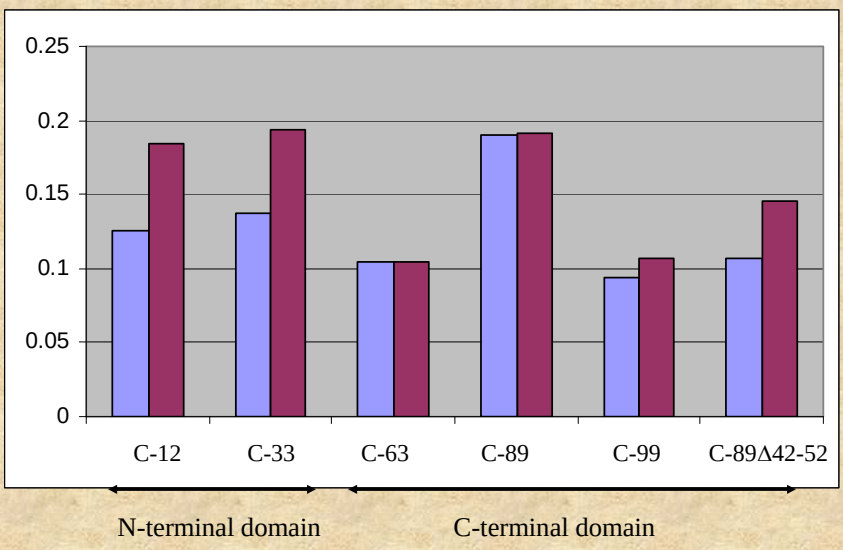

These changes in polarization due to homoFRET allow us to assign maximum proximity values for the C-terminal domains.

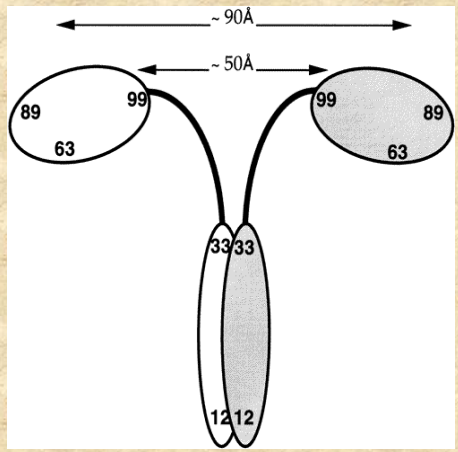

The conclusion is that the C-terminal domains are well-separated – contrary to the original model from the X-ray studies and the usual depictions in the literature

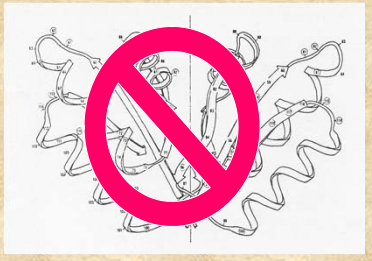

Homo-FRET Microscopy in Living Cells to Measure Monomer-Dimer Transition of GFP-Tagged Proteins

I. Gautier,* M. Tramier,* C. Durieux,* J. Coppey,* R. B. Pansu,† J-C. Nicolas,‡ K. Kemnitz,§ and M. Coppey-Moisan*

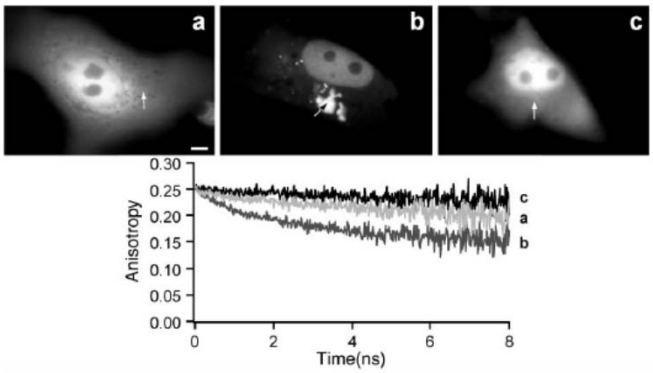

FIGURE 1 Subcellular fluorescence anisotropy decays of TK_{27}GFP and TK_{366}GFP proteins. (*Top*) Steady-state fluorescence images of Vero cells expressing TK_{27}GFP (*a*) and TK_{366}GFP (*b* and *c*). (*a* and *c*) Cells presenting only a diffuse cytoplasmic and nuclear fluorescence pattern; (*b*) Cells containing fluorescent aggregates. (*Bottom*) Time-resolved fluorescence depolarization from a cytoplasmic area of diffuse fluorescence (*a* and *c*) and from an area inside an aggregate (*b*). The subcellular location of the illuminated volume (~1 μm^3) from which the anisotropy decay was performed is indicated by an arrow. For cells containing aggregates, anisotropy decays from nuclear or cytoplasmic area of diffuse fluorescence were similar to that obtained from aggregates (*b*). Bar in *a*, 5 μm.

Biophys J, June 2001, p. 3000-3008, Vol. 80, No. 6

Other examples of homo-FRET *in vivo* can be found in: Tramier et al., 2003 "Homo-FRET versus hetero-FRET to probe homodimers in living cells" Methods Enzymol. 360:580-97.

To summarize this lecture is not intended to prepare you to start FRET measurements immediately but rather to make you aware of the salient principles and pitfalls

Several books on this topic are available as well as MANY articles in the primary literature

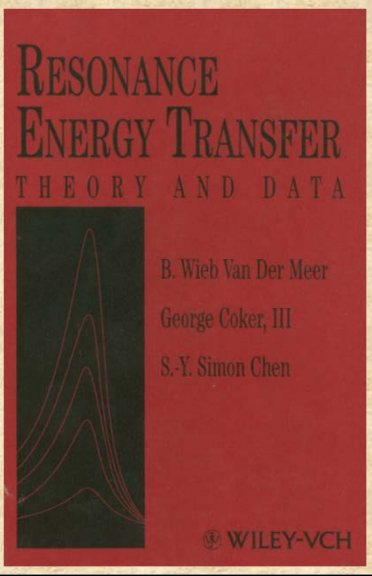

Fluorescence Probes

In vitro *(or In Silico)*

In vivo (or more accurately in cells)

Some of these slides were prepared by
Susana Sanchez
and
Ewald Terpetschnig

Classification:

- Intrinsic Fluorophores
- Extrinsic Fluorophores

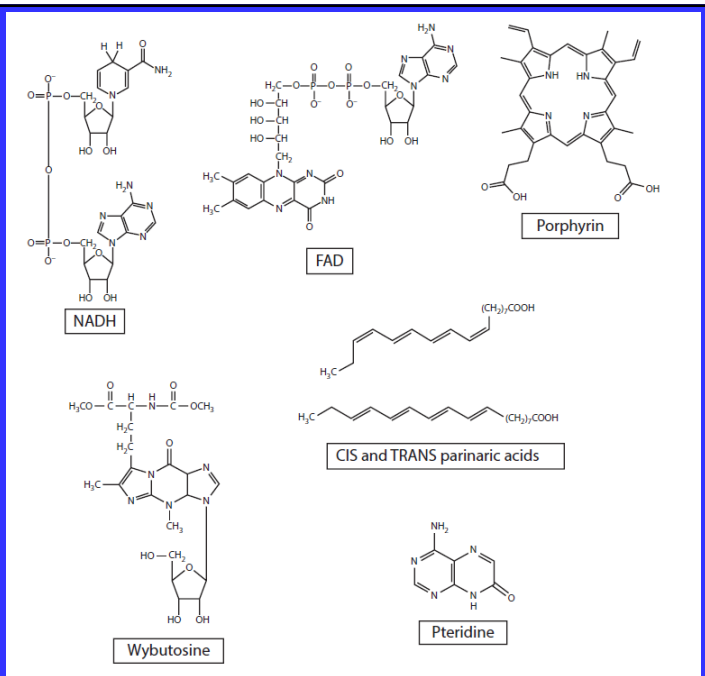

FIGURE 10.2 Structures of several intrinsically fluorescent biomolecules.

Proteins: Naturally Occurring Fluorophores

Aromatic amino acids

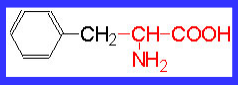

Phenylalanine (Phe – F)
Ex/Em 260 nm/282 nm

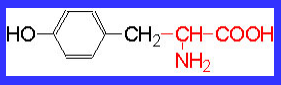

Tyrosine (Tyr – Y)
Ex/Em 280 nm/303 nm

Tryptophan (Trp-W)
Ex/Em 280, 295nm/ 305-350 nm

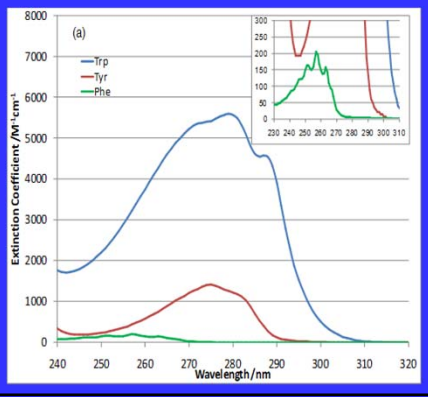

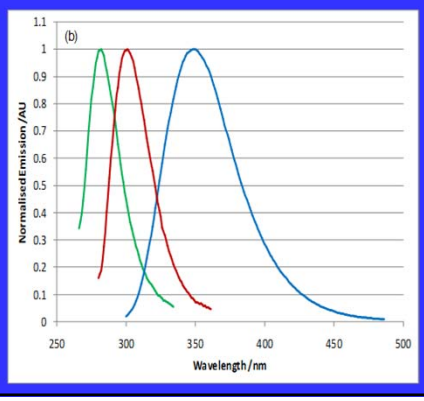

Tryptophan derivatives

Tryptophan derivatives may be genetically incorporated in a protein

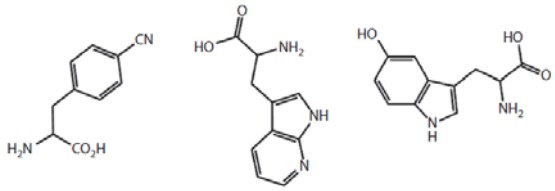

p-cyanophenylalanine

7-azatryptophan

5-hydroxytryptophan

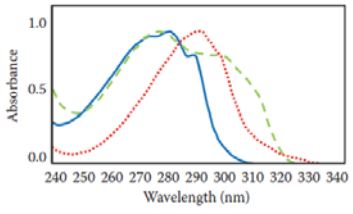

FIGURE 11.13 Structures of *p*-cyanophenylalanine, 7-azatryptophan, 5-hydroxytryptophan, and absorption spectra of tryptophan (blue solid line), 7-azatryptophan (red dotted line), and 5-hydroxytryptophan (green dashed line).

Extrinsic Fluorophores

Synthetic dyes or modified biochemicals that are added to a specimen to produce fluorescence with specific spectral properties

Fluorescent Probes:

- Non covalent interactions

  A fluorescent probe is a fluorophore designed to localize within a specific region of a biological specimen or to respond to a specific analyte.

- Covalent interactions

Extrinsic probes

(not present in the natural molecule/macromolecule)

Non-covalent Attachment

Barely fluorescent in pure water but their fluorescence can be strongly enhanced if the environment becomes hydrophobic (hydrophobic patches on proteins)

1,8-ANS

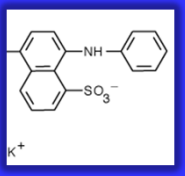

bis-ANS

2,6 TNS

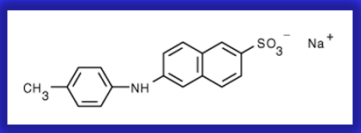

Fluorescent Probes

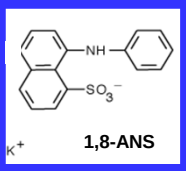

1,8-ANS

Non-covalent

1,8-ANS

Developed by G. Weber in the early 1950's

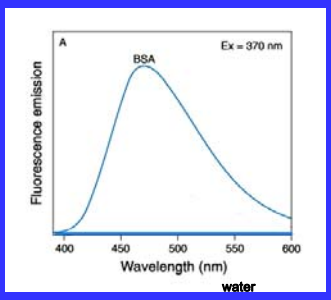

Barely fluorescent in water - fluorescence is strongly enhanced in hydrophobic environments

It is interesting to note that even today, more than 50 years after that first report, ANS is still being used in protein studies, quite often as an indicator of the "molten globular" state.

Water BSA

Other probes, which bind to some proteins noncovalently, include thioflavin T and Congo Red (**Figure 10.15**), dyes, which have become extremely popular for following amyloid fiber formation. Thioflavin T exhibits shifts in its excitation and emission spectra and a significant increase in its quantum yield upon binding to amyloid-type protein. When Congo Red interacts with amyloid fibrils, its absorption maximum shifts from about 490 to 540 nm. Nile Red (**Figure 10.15**), although primarily known as a lipid probe, also binds to hydrophobic regions of some proteins and has been used to study protein aggregation and denaturation.

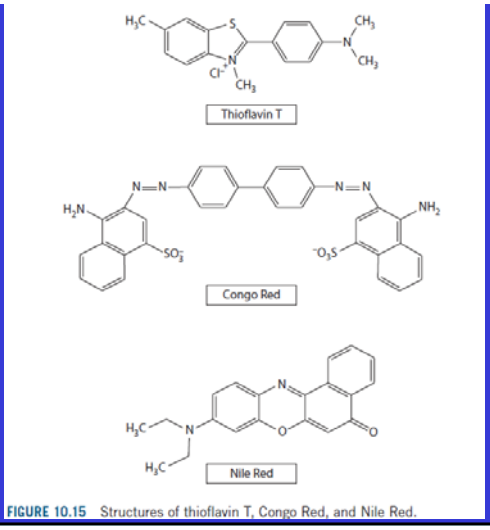

FIGURE 10.15 Structures of thioflavin T, Congo Red, and Nile Red.

Extrinsic probes for covalent attachment

The first extrinsic probe (at least the first one to achieve widespread use) was fluorescein, made in 1871 by Adolf von Bayer (as mentioned in Chapter 1). The first extrinsic fluorescein label was made by Albert Coons and his colleagues in 1941, who labeled antibodies with fluorescein isocyanate, thus giving birth to the field of immunofluorescence. J. L. Riggs and colleagues first reported the synthesis of fluorescein isothiocyanate (FITC; **Figure 10.3**) in 1958, which they synthesized to circumvent problems inherent in the isocyanate derivative, including the difficulty of its synthesis and its instability. FITC became, arguably, the most popular fluorescent label of all time. I note that FITC is available in two common isomers; isomer 1 or 2, which have the isothiocyanate group on carbon 4 or 5 of the benzene ring, respectively. Isomer 1 is easier to purify and hence, is usually less expensive.

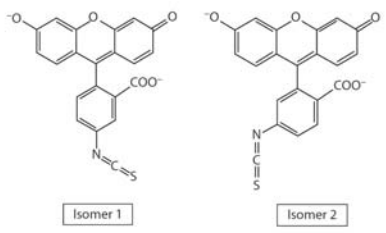

FIGURE 10.3 Structures of fluorescein isothiocyanate (FITC) isomer 1 and isomer 2.

By 1951, Gregorio Weber had begun to develop methods which would allow him to study proteins not containing intrinsic fluorophores such as FAD or NADH (the fluorescence of the aromatic amino acids had not yet been discovered). To this end, he invested considerable time and effort in synthesizing a fluorescent probe, which could be covalently attached to proteins and which possessed absorption and emission characteristics appropriate for the instrumentation available in post-war England. The result of two years of effort was the still popular probe 1,5-dimethylaminonaphthalene sulfonyl chloride or dansyl chloride (**Figure 10.4**). Using this probe, Weber initiated the field of quantitative biological fluorescence.

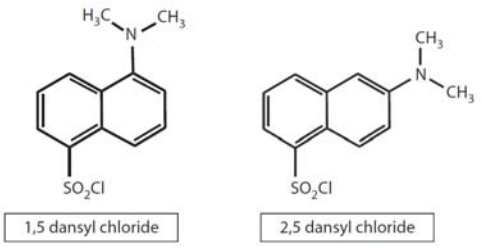

FIGURE 10.4 Structures of 1,5- (and 2,5-) dimethylaminonaphthalene sulfonyl chloride (dansyl chloride).

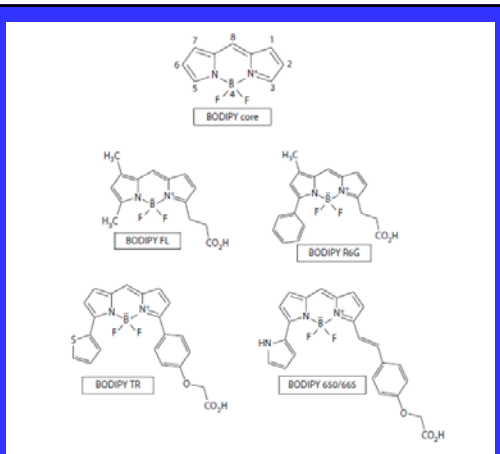

FIGURE 10.7 Structures of several BODIPY probes, including the core structure with the ring numbering.

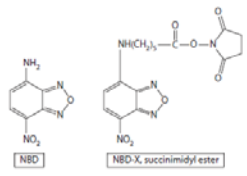

FIGURE 10.8 Structure of NBD and NBD-X, a succinimidyl ester of NBD.

The Alexa-Fluor series

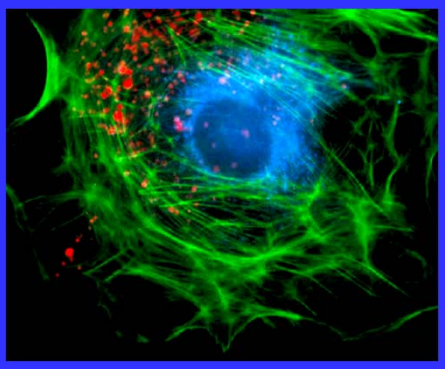

1999
"there is a need
for probes with high fluorescence quantum yield and high photostability to allow detection of low-abundance biological structures with great sensitivity and selectivity"

The Journal of Histochemistry & CytochemistryVolume 47(9): 1179–1188, 1999.Molecular Probes, Inc., Eugene, Oregon

Designed to be more photostable than their commonly used spectral analogues

Coumarin-AMCA → **Alexa 350** 346/442

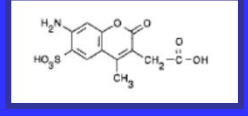

Lucifer Yellow → **Alexa 430** 434/539

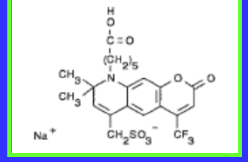

fluorescein → **Alexa 488** 495/519

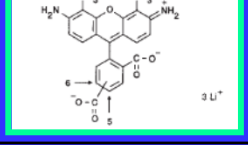

rhodamine 6G → **Alexa 532** 531/554

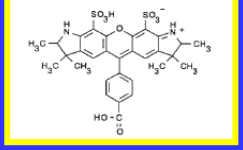

lissamine rhodamine B → **Alexa 568** 578/603

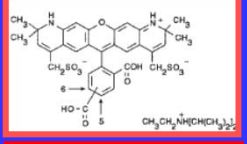

Texas Red → **Alexa 594** 590/617

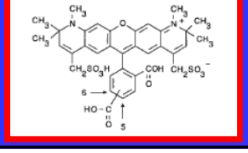

All Alexa dyes and their conjugates are more fluorescent and more photostable than their commonly used spectral analogues.

In addition, Alexa dyes are insensitive to pH in the 4–10 range.

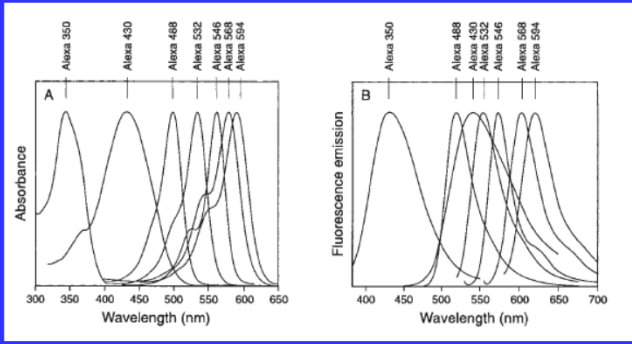

The Journal of Histochemistry & CytochemistryVolume 47(9): 1179–1188, 1999.
Molecular Probes, Inc., Eugene, Oregon

Photostability
Alexa Fluor 488 v/s fluoresceine

Photo bleaching profile

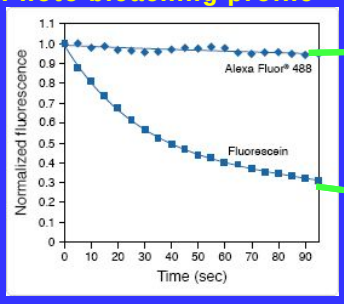

Alexa 488

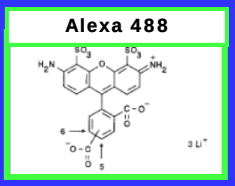

FLUORESCEIN

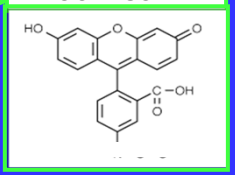

- Cells stained with Alexa Fluor488 or fluorescein conjugates of goat anti–mouse IgG antibody

- Samples were continuously illuminated and images were collected every 5 seconds with a cooled CCD camera.

http://www.invitrogen.com/

The Alexa series expanded

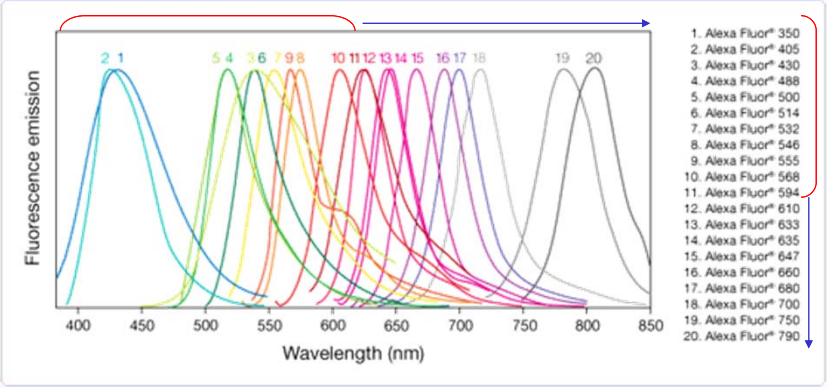

Alexa Fluor dyes are available as amine-reactive succinimidyl esters

Fluorescence quantum yields (QY) and lifetimes (τ) for Alexa Fluor dyes–

Alexa Fluor Dye *	QY †	τ (ns) ‡
Alexa Fluor 488	0.92	4.1 §
Alexa Fluor 532	0.61	2.5
Alexa Fluor 546	0.79	4.1
Alexa Fluor 555	0.10	0.3
Alexa Fluor 568	0.69	3.6 §
Alexa Fluor 594	0.66	3.9 §
Alexa Fluor 647	0.33	1.0
Alexa Fluor 660	0.37	1.2 **
Alexa Fluor 680	0.36	1.2
Alexa Fluor 700	0.25	1.0
Alexa Fluor 750	0.12	0.7

http://www.invitrogen.com

Cyanine dyes (available from Lumiprobe (www.lumiprobe.com) and GELifeSciences (www.gelifesciences.com), sometimes known as indocyanine dyes, were first synthesized over a century ago and are also known for their photostability. Cy3 and Cy5 probes, among the most popular cyanine dyes, are shown in **Figure 10.10**. Variation of the R-groups in these structures gives rise to a wide family of fluorophores and chemical functionalities. The cyanine dye Cy3B, shown in **Figure 10.10**, has a rigid backbone in place of the open chain trimethine of Cy3 and has a significantly higher quantum yield (~0.67 versus ~0.04) and lifetime (~2.8 ns versus ~0.3 ns) compared to Cy3.

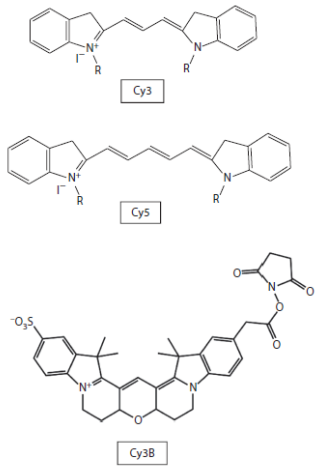

FIGURE 10.10 Structures of several cyanine dyes.

Protein Labeling

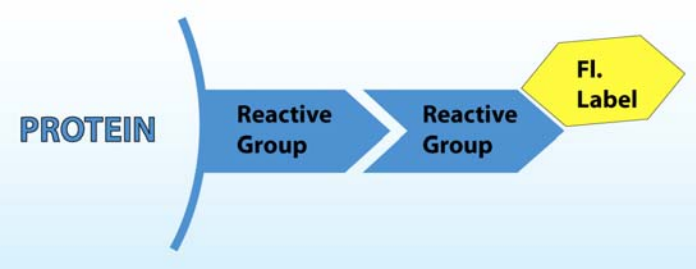

Reactive groups on proteins

- NH_2 Lysine N-terminus
- SH Cysteine

Depends on the reactive group on the protein

Light source

Spectral properties

Autofluorescence

Photostability

Labeling should not alter the biological activity of biomolecules

Protein Labeling

Amino-Modification:

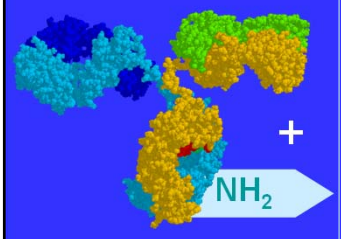

Protein-NH_2

Lysine
N-terminus

isothiocyanate:
Fl-N=C=S
→ Fl-NH-C(=S)-NH-Protein
Thiourea

succinimidyl ester:
Fl-C(=O)-O-N(succinimide)
→ Fl-C(=O)-NH-Protein
Carboxamide
+ HON(succinimide)

sulfonyl chloride:
$Fl\text{-}SO_2Cl$
→ $Fl\text{-}SO_2\text{-}NH\text{-}Protein$
Sulfonamide
+ HCl

aldehyde:
Fl-CH=O
→ Fl-CH=N-Protein
Schiff Base
→ reduction

Protein Labeling

Thiol-Modification:

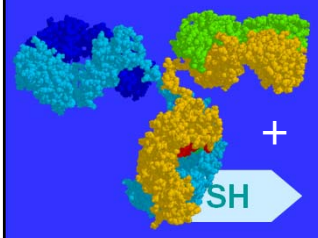

Protein-SH

Cysteine

X-CH_2-C(=O)-NH-Fl
alkyl halides or
iodoacetamides
→ Protein-S-CH_2-C(=O)-NH-Fl
Thioether

Fl-N(maleimide)
Maleimide
→ Fl-N(succinimide)-S-Protein
Thioether

Click Chemistry

In recent years, the method known as "click chemistry," developed largely by K. Barry Sharpless, has been recognized as an important advance in synthetic organic chemistry, and is now being used in the attachment of fluorophores to target molecules. Click chemistry relies on an azide–alkyne Huisgen cycloaddition reaction, the most popular being a copper (I)-catalyzed azide–alkyne cycloaddition. Basically, an azide and an alkyne react to form a triazole, which forms a stable covalent bond, as illustrated in **Figure 10.21**. Click chemistry "ready" fluorescent reagents are now available commercially (see, e.g., www.setabiomedicals.com, www.jenabioscience.com, and www.activemotif.com).

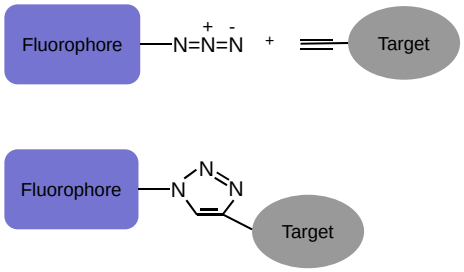

FIGURE 10.21 Example of a click chemistry reaction.

Photoaffinity Labeling

Affinity labels are reagents specifically designed to bind with high affinity to a biomolecule, for example, a protein, nucleic acid, or membrane. They are often analogs of substrates or inhibitors. The photoactivatable moiety is typically an azide group or a benzophenone, although other chemistries are available. A useful design is shown in **Figure 10.22**, which comprises a fluorescent moiety (fluorescein), a photoactivatable moiety (aryldiazirine) and an affinity ligand (a sidechain portion of aplyronine A). Such photoaffinity reactions are typically carried out using UV illumination, often from the 366 nm line of a standard UV handlamp.

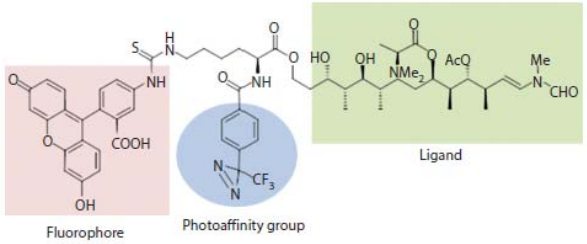

FIGURE 10.22 Example of a photoactivatable probe comprising a fluorescent moiety (fluorescein), a photoactivatable moiety (aryldiazirine) and an affinity ligand (a sidechain portion of aplyronine A). (Modified from Kuroda et al., 2006. *Bioconjugate Chem.* 17: 524.)

Labeling Procedure

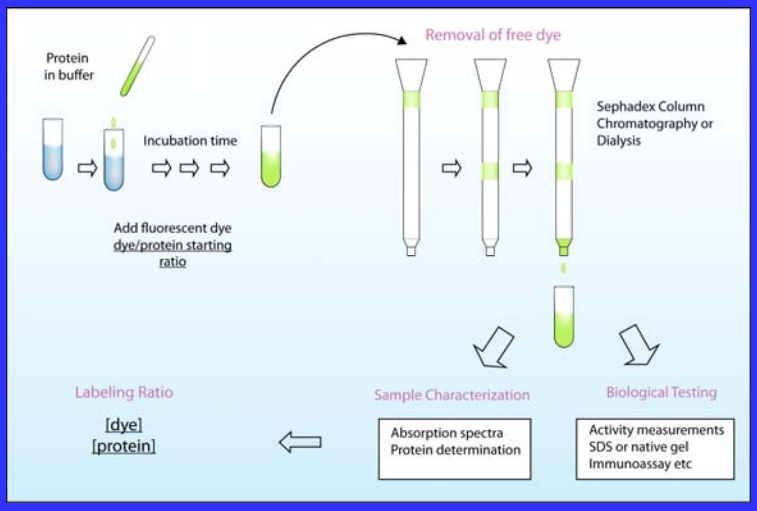

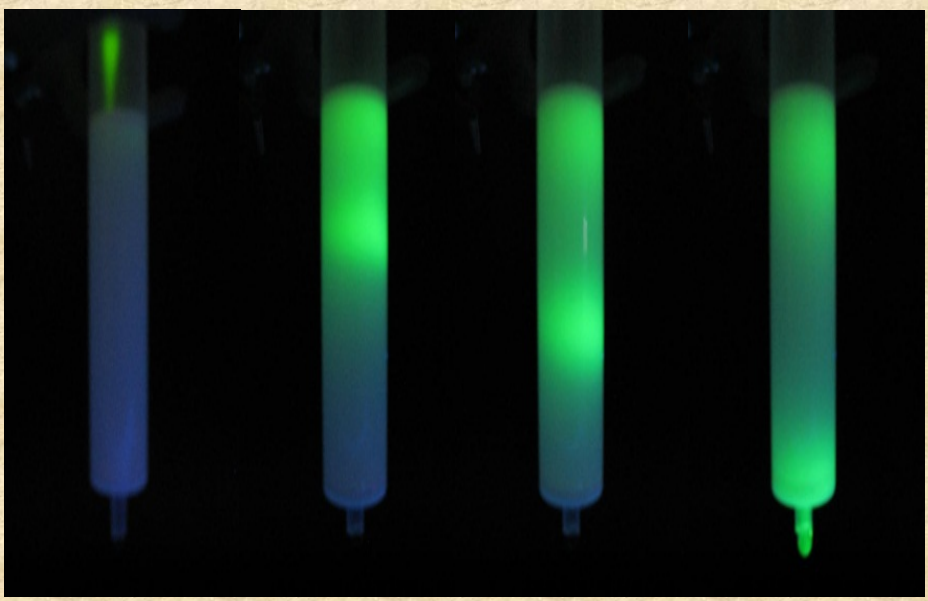

Characterization after the labeling

Protein-Fluorescein

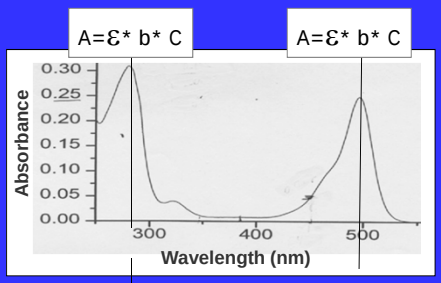

Fluorescein

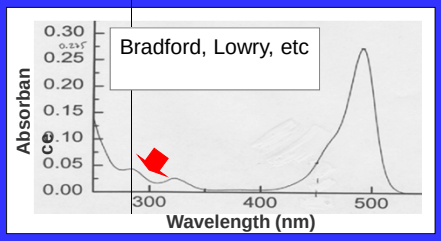

Labeling should not change the biological activity of the protein.

Labeling membranes

- Analogs of fatty acids and phospholipids
- Di-alkyl-carbocyanine and Di-alkyl-aminostyryl probes.
- Other nonpolar and amphiphilic probes.
  DPH, Laurdan, Prodan, Bis ANS

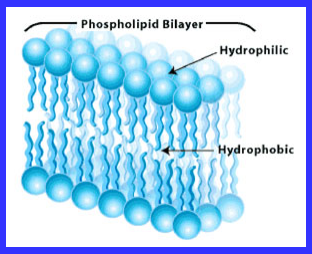

Membrane Probes

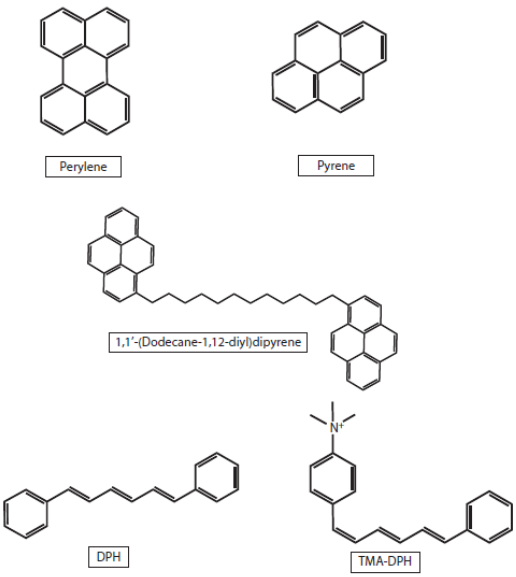

FIGURE 10.25 Structures of various membrane probes.

DPH - diphenylhexatriene

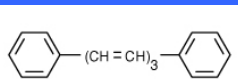

THE JOURNAL OF BIOLOGICAL CHEMISTRY
Vol. 249, No. 8, Issue of April 25, pp. 2652-2657, 1974
Printed in U.S.A.

Dynamics of the Hydrocarbon Layer in Liposomes of Lecithin and Sphingomyelin Containing Dicetylphosphate*

(Received for publication, September 12, 1973)

MEIR SHINITZKY AND YECHEZKEL BARENHOLZ

From the Department of Biophysics, The Weizmann Institute of Science, Rehovot, Israel, and the Department of Biochemistry, The Hebrew University-Hadassah Medical School, Jerusalem, Israel

SUMMARY

Physical properties of the hydrocarbon region in lipid bilayers were studied in a series of liposomes of lecithin and sphingomyelin containing different concentrations of dicetylphosphate. The technique used was described previously and is based on fluorescence polarization analysis of a specific probe embedded in the analyzed region. The two probes employed in this study were perylene and 1,6-diphenyl-1,3,5-hexatriene, which simulate a rotating disc and a rotating rod, respectively. The determined dynamic properties of the hydrocarbon region in the lecithin liposomes differ markedly from those of the sphingomyelin liposomes. The hydrocarbon region of the lecithin liposomes is of an invariant phase between 0° and 60° characterized by a microviscosity at 25°, $\bar{\eta}$ (25°), of 0.8 ± 0.1 poise and a fusion activation energy, ΔE, of 8 ± 2 Cal per mole. In contradistinction to lecithin, the hydrocarbon region of the sphingomyelin liposomes displays a distinct phase transition at 32° ± 2°. The phase at temperatures above the transition point, presumably a liquid crystalline phase, is characterized by ΔE = 16 ± 4 Cal per mole, whereas the phase below it, presumably a gel state, possesses a ΔE value lower than 3 Cal per mole. In addition to that, the hydrocarbon layer in sphingomyelin liposomes is much more viscous than in lecithin liposomes as shown by $\bar{\eta}$ (25°) = 6 ± 1 poise. All of the above characteristics are only slightly and irregularly affected by the presence of dicetylphosphate, despite the strong effects it exerts on the surface charge potential of the liposomes. This indicates that the forces which dictate the dynamic properties of the hydrocarbon region in lipid bilayers predominantly originate from hydrophobic interactions.

different and specific value for each mammalian species. In some membranes this ratio changes drastically with age (1, 2).

The molecular structure of sphingomyelin and lecithin can be separated into two distinct regions: the hydrophilic region, which contains the phosphorylcholine moiety in both lipids, and the hydrophobic region, which contains the hydrocarbon chains. In addition to the phosphorylcholine group, the polar region of lecithin contains two ester bonds, whereas that of sphingomyelin contains an amide bond, an hydroxyl group, and a *trans* double bond. These groups result in difference in the net dipole moment and in the ability to form hydrogen bonds (3, 4). In the hydrophobic region the average length of the hydrocarbon chains in lecithin is shorter and the degree of unsaturation is greater than in sphingomyelin (1). The special nature of these regions in sphingomyelin and lecithin is therefore expected to exert specific effects on structure and dynamics of lipid layers.

In this study, structure and dynamic properties of sonicated liposomes, made of sphingomyelin or lecithin containing dicetylphosphate, were investigated. The method employed was described previously (5, 6) and is based on determination of fluorescence polarization of a hydrocarbon probe and translating it into microviscosity, $\bar{\eta}$, which is obtained in absolute macroscopic units (*e.g.* poise). From the temperature profile of $\bar{\eta}$ phase transitions were detected and the fusion activation energies, ΔE, of each phase were determined (5, 6).

EXPERIMENTAL PROCEDURES

Phospholipids—Lecithin was prepared from egg yolks (7) and purified chromatographically on alumina and silica columns (8). For chemical analysis lecithin was first hydrolyzed by mild alkali (0.4 N KOH in 90% methanol for 2 hours at 37°) and the fatty acids were extracted and methylated with diazomethane. The methyl esters were then analyzed with a Packard gas-liquid chromatograph on 15% ethylene glycol succinate column. The obtained

Fatty acids analogs and phospholipids

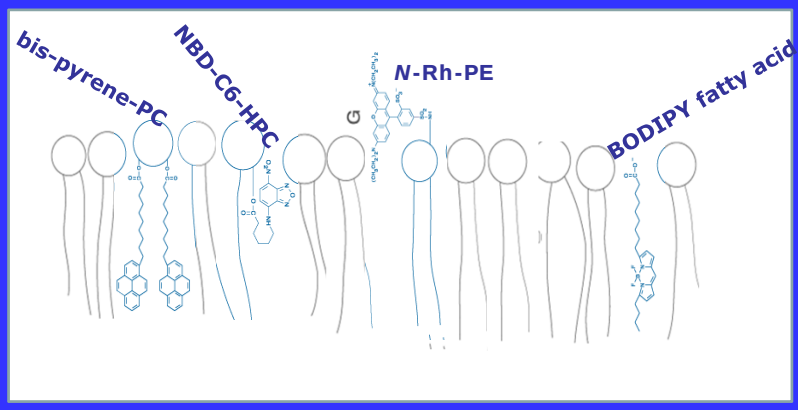

Pyrene (**Figure 10.25**) has also been widely used in membrane studies because of its ability to form excited dimers or *excimers*. Formation of an excimer requires that an excited pyrene molecule can form a complex with a ground state pyrene—which, of course, must occur during the lifetime of the excited state. Since pyrene excited states tend to be long (tens or hundreds of nanoseconds depending on the exact probe), the likelihood of such an encounter is reasonable if the concentration of the probe is sufficient and if the medium, in this case a biological membrane, is sufficiently fluid to ensure facile diffusion of the fluorophores. The excimer emission is red-shifted from the monomer emission so one simply has to determine the ratio of excimer to monomer emission to quantify the extent of excimer formation. An example of the use of pyrene excimers is shown in **Figure 10.26**. In this example, an aptamer probe for platelet-derived growth factor (PDGF) was synthesized with one pyrene molecule at each end. In the absence of the target protein, the aptamer adopts an open conformation such that each pyrene molecule is free to emit as a monomer (emission in the 350–440 nm range). When bound to the PDGF, however, the two pyrenes come into proximity and are able to emit as an excimer (emission above 440 nm). The increase in the excimer to monomer emission allows one to track the formation of the aptamer–PDGF complex. One can also use pyrene probes which contain two pyrene molecules connected by a linker. These types of dual probes have the advantage that both potential excimer partners are in the same molecule—hence, eliminating the requirement for the high probe concentrations necessary to ensure diffusional contact during the fluorescent lifetime.

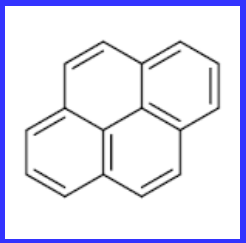

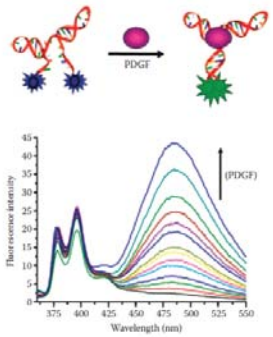

FIGURE 10.26 Example of the use of pyrene excimers. (Adapted from Yang et al., 2005. *Proc. Natl. Acad. Sci. USA* 102: 17278.) An aptamer probe for platelet-derived growth factor (PDGF) has one pyrene molecule at each end. In the absence of the target protein, the aptamer adopts an open conformation such that each pyrene molecule is free to emit as a monomer (emission in the 350–440 nm range). When bound to the PDGF, however, the two pyrenes come into proximity and are able to emit as an excimer (emission above 440 nm).

Nonpolar probes

Environment-sensitive spectral shifts

Weber, G. and Farris, F. J.Biochemistry, 18, 3075-3078 (1979) .

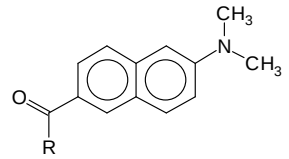

LAURDAN R = $-(CH_2)_{10}CH_3$

PRODAN R = $-CH_2CH_3$

DANCA R = 

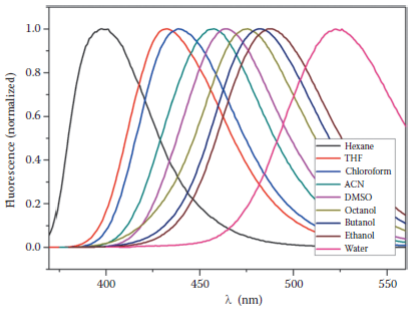

FIGURE 10.29 Emission spectra for Prodan in a series of solvents. The author would like to thank Leonel Malacrida for these spectra.

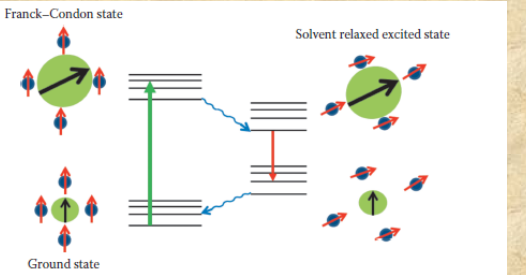

FIGURE 10.27 Depiction of excited state solvent reorientation (dipolar relaxation).

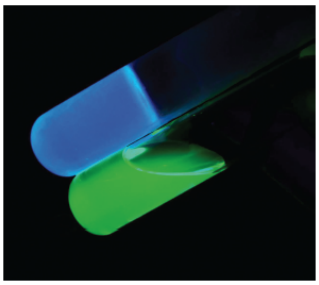

FIGURE 10.28 Prodan in glycerol at –80°C (top blue tube) and +60°C (bottom green tube) illuminated using a UV handlamp.

Nonpolar probes (continued)

example: ***Laurdan.***

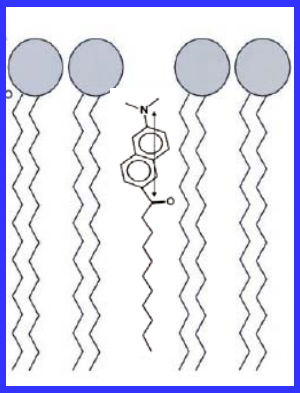

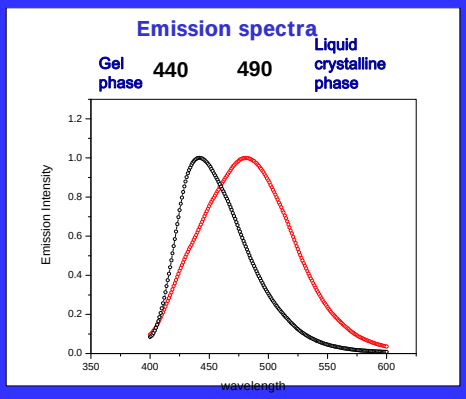

Laurdan Generalized Polarization (GP)

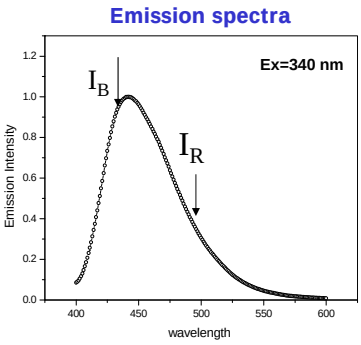

$$GP_{ex} = \frac{I_B - I_R}{I_B + I_R}$$

-0.2 loose lipid packing → 0.6 tight lipid packing

Parasassi et al. Biophysical J., 60, 179-189 (1991).

GP in the cuvette

MLVs, SUVs, LUVs

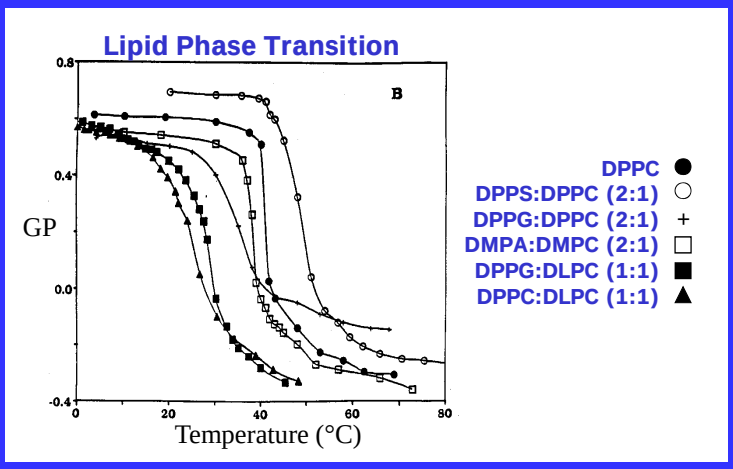

Parassassi et al. Biophys. J. 60, 179 (1991)

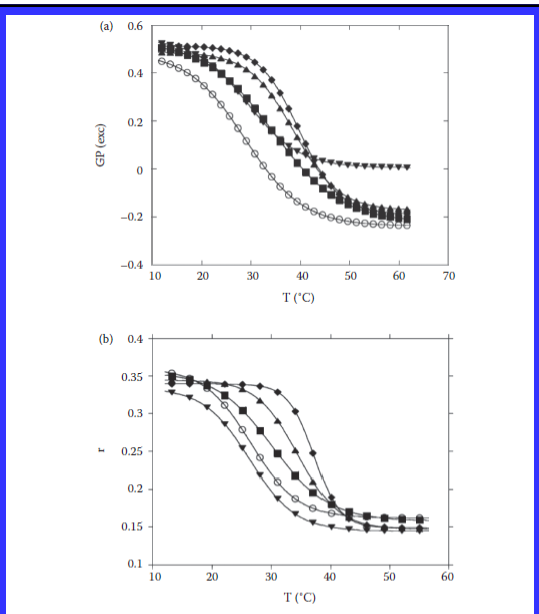

FIGURE 10.33 Example of the use of Laurdan's GP values to monitor phase transitions in a model membrane system. The figure, from Deleu et al., 2013. (*Biochim. Biophys. Acta* 1828: 801), presents a comparison of (a) Laurdan GP with (b) DPH anisotropy in the same system, specifically, DOPC:DPPC large unilamaellar vesicles with increasing concentrations of surfactin.

GP in the microscope
(2-photon excitation)

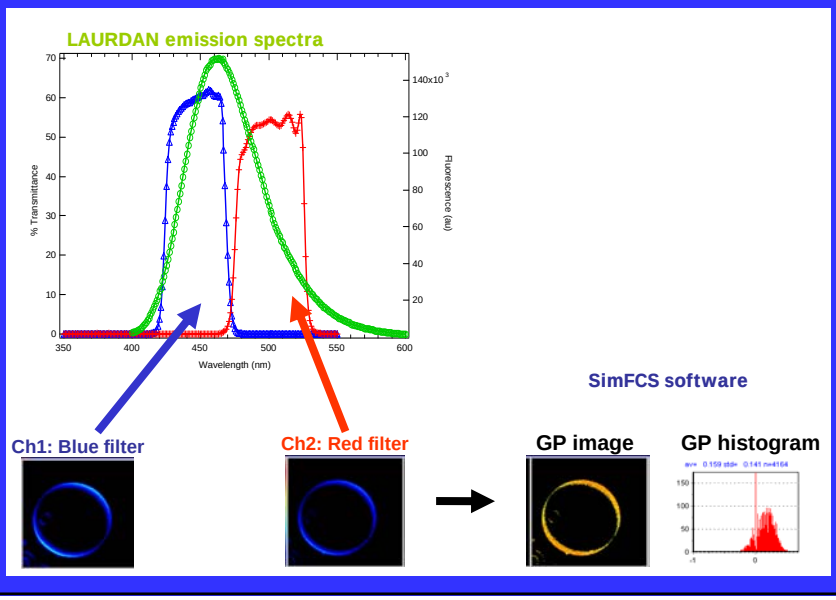

Fluorescent Ion-Probes

Fluorescence probes have been developed for a wide range of ions:

Cations:

H^+, Ca^{2+}, Li^+, Na^+, K^+, Mg^{2+}, Zn^{2+}, Pb^{2+} *and others*

Anions:

Cl^-, PO_4^{2-}, Citrate, ATP, *and others*

Probes For Calcium determination

UV
FURA
(Fura-2, Fura-4F, Fura-5F, Fura-6F, Fura-FF)
INDO
(Indo-1, Indo 5F)

Ratiometric

VISIBLE
FLUO
(Fluo-3, Fluo-4, Fluo5F, Fluo-5N, Fluo-4N)
RHOD (Rhod-2, Rhod-FF, Rhod-5N)
CALCIUM GREEN (CG-1, CG-5N,CG-2)
OREGON GREEN 488-BAPTA

Non Ratiometric

Ratiometric: 2 excitation / 1emission

FURA-2

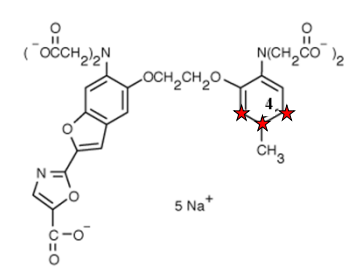

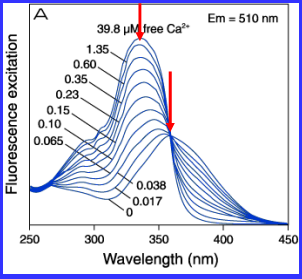

Indicator	$K_d(Ca^{2+})$
Fura-2	0.14 μM
Fura-5F	0.40 μM
Fura-4F	0.77 μM
Fura-6F	5.30 μM
Fura-FF (5,6)	35 μM

Most used in microscopic imaging

Good excitation shift with Ca^{2+}

Rationed between 340 / 350 and 380 / 385 nm

Ratiometric: 1excitation / 2emission

Indo-1

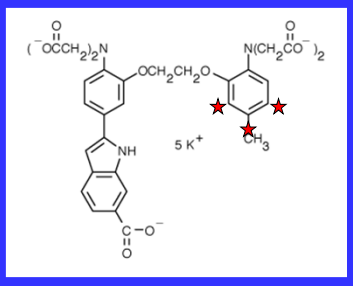

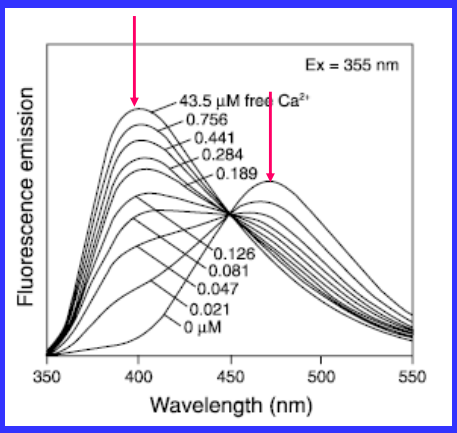

Indicator	K_d (Ca^{2+}) (µM)
indo-1	0.23
indo-5F	0.47

CalciumGreen-5N

Non-Ratiometric

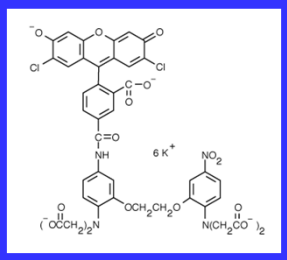

Fluorescence Intensity

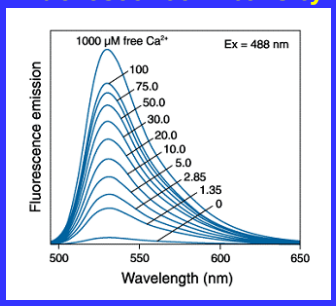

Fluorescence Lifetime

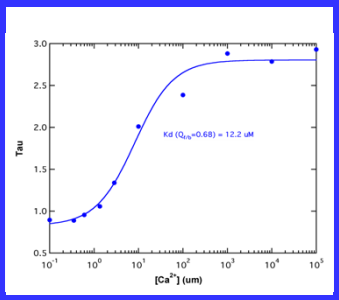

pH-Probes

Probe	pH Range	Measurement Mode
SNARF indicators	6.0-8.0	Em. ratio 580/640 nm
HPTS (pyranine)	7.0-8.0	Exc. ratio 450/405 nm
BCECF	6.5-7.5	Exc. ratio 490/440 nm
Fluoresceins and Carboxyfluoresceins	6.0-7.2	Exc. ratio 490/450 nm
Oregon Green dyes	4.2-5.7	Exc. ratio 510/450 nm
LysoSensor Yellow/Blue DND-160	3.5-6.0	Em. ratio 450/510 nm

Molecular Probes' pH indicator families, in order of decreasing pK_a

BCECF

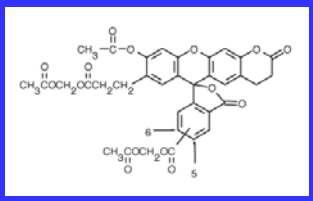

R. Tsien 1982

Most widely used fluorescent indicator for intercellular pH

Membrane-permeant AM: pKa ~ 6.98 is ideal for intracellular pH measurements

Excitation-ratiometric probe with Ip at 439 nm, which is used a the reference point

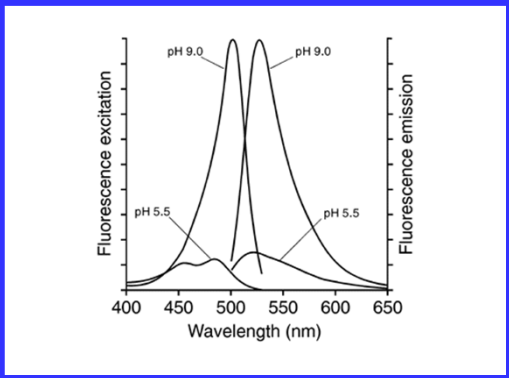

Quantum Dots

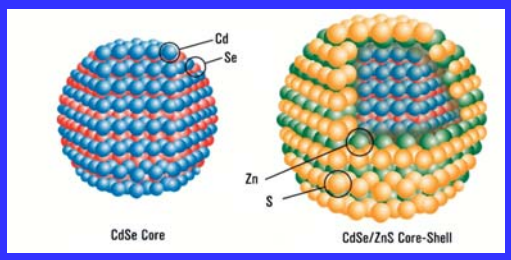

Quantum Dots

Nanometer-Scale Atom Clusters

CORE

Cadmium selenide (**CdSe**), or Cadmium telluride (**CdTe**)
few hundred – few thousand atoms

The semiconductor material is chosen based upon the emission wavelength, however it is the **size** of the particles that **tunes the emission wavelength**.

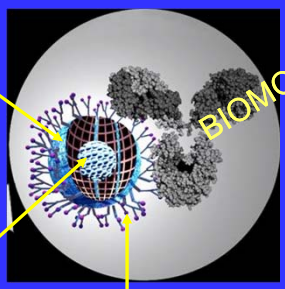

SHELL

In the core emission is typically weak and always unstable.
The shell material (**ZnS**) has been selected to be almost entirely unreactive and completely insulating for the core.

COATING

A layer of organic ligands covalently attached to the surface of the shell. This coating provides a **surface for conjugation** to biological (antibodies, streptavidin, lectins, nucleic acids) and nonbiological species and makes them "water-soluble"
.

Quantum Dots

Nanometer-Scale Atom Clusters

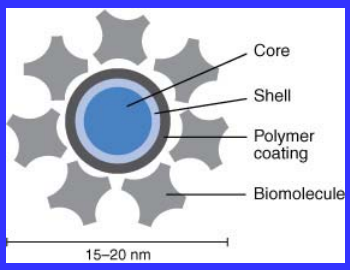

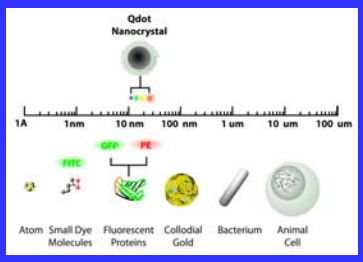

Quantum Dot Material System	Emission Range	Quantum Dot Diameter Range	Quantum Dot Type	Standard Solvents	Example Applications
CdSe	465nm - 640nm	1.9nm - 6.7nm	Core	Toluene	Research, Solar Cells, LEDs
CdSe/ZnS	490nm - 620nm	2.9nm - 6.1nm	Core-Shell	Toluene	VisibleFluorescence Applications, Electroluminescence, LEDs
CdTe/CdS	620nm - 680nm	3.7nm - 4.8nm	Core-Shell	Toluene	Deep Red Fluorescence Apps.

Qdot Optical Spectra

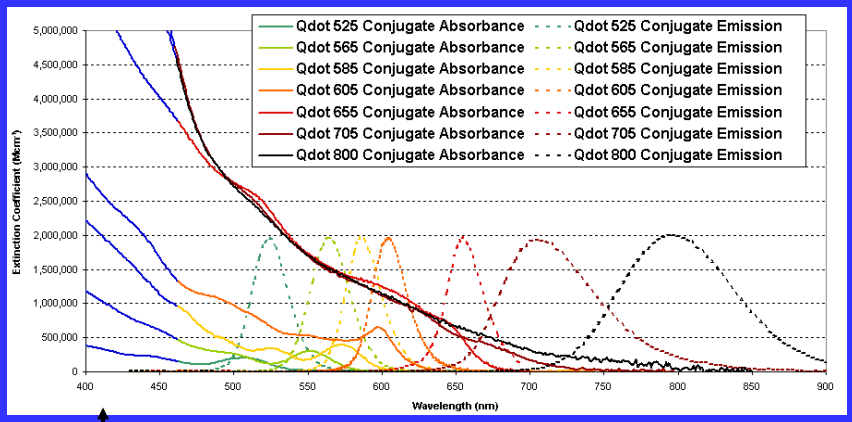

Violet excitation

Absorbance × Quantum Yield = Brightness

photons in **fraction converted** **photons out**

Broad range of emissions

High absorbance means increased brightness

Single-color excitation, multicolor emission for easy multiplexing

Courtesy of Invitrogen

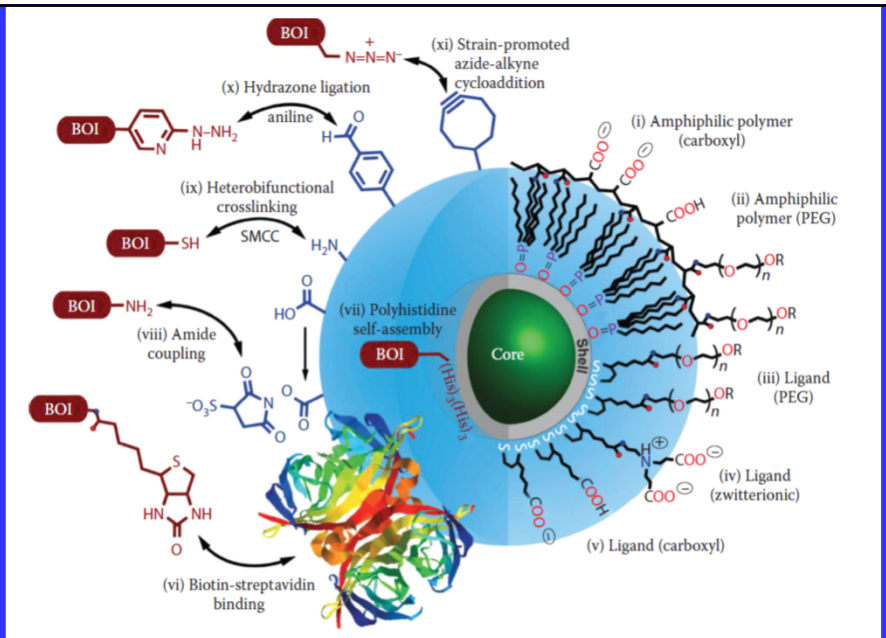

FIGURE 10.57 Illustration of functionalization strategies for Q-dots. (From Petryayeva et al., 2013 *Appl. Spectros.* 67: 215.)

Qdot Summary

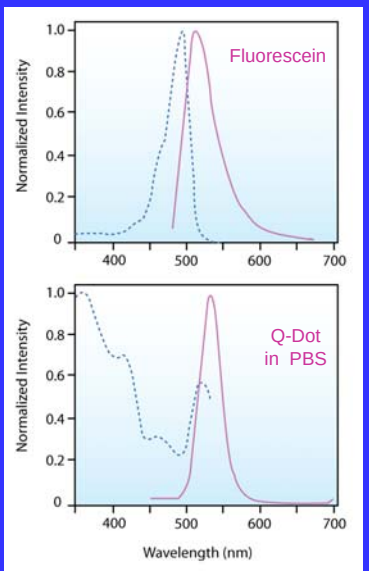

Advantages:

Broad absorption spectra, making it possible to excite all colors of QDs simultaneously with a single light source - **Multiplexing**

Narrow and symmetrical emission spectra

Emission tunable with size and material composition

Exhibit excellent **photo-stability**

Disadvantages:

Large size and **high mass** limit their use in applications requiring high diffusional mobility

QDot	$\lambda_{max\ (abs)}$ [nm]	$\lambda_{max\ (em)}$ [nm]	ε ($M^{-1}cm^{-1}$)	Q.Y.
655	350	655	9,000,000	~0.5
705	350	705	13,000,000	~0.5
800	350	800	13,000,000	~0.5

Green Fluorescent Protein

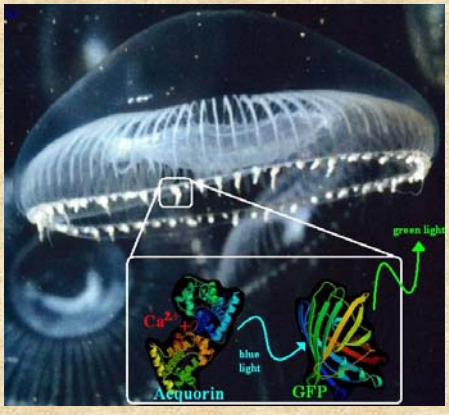

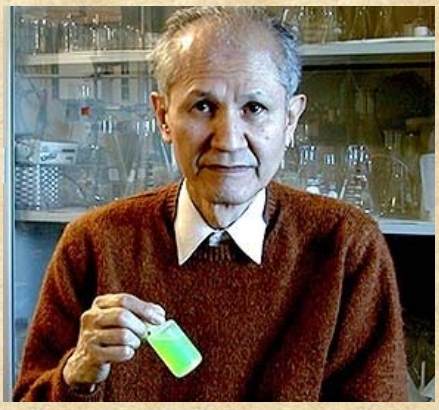

Aequorea victoria jellyfish

Osamu Shimomura

Shimomura O, Johnson F, Saiga Y (1962). "Extraction, purification and properties of aequorin, a bioluminescent protein from the luminous hydromedusan, Aequorea". *J Cell Comp Physiol* **59**: 223-39.

"The jellyfish *Aequorea* and its light-emitting organs"

O. SHIMOMURA:*Journal of Microscopy, Vol. 217, Pt 1 January 2005, pp. 3–15*

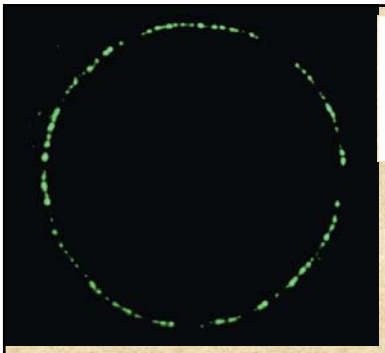

Intermolecular Energy Transfer in the Bioluminescent System of *Aequorea*†

Hiroshi Morise, Osamu Shimomura, Frank H. Johnson,* and John Winant

2656 BIOCHEMISTRY, VOL. 13, NO. 12, 1974

Materials and Methods

Aequorin. The material used in this study was extracted and purified from some 30,000 specimens of *Aequorea*

70 mgs of purified GFP were obtained.
The 30,000 jellyfish weighed about 1.5 tons

The outer ring of the jellyfish had to be isolated. Intially scissors were used but then a "ring-cutting" machine was built

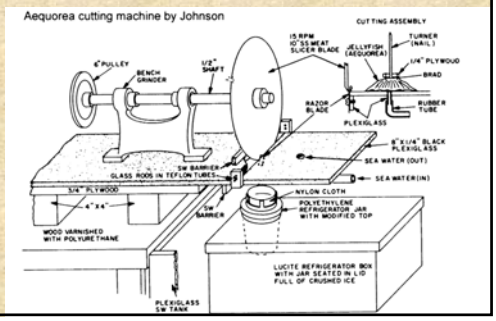

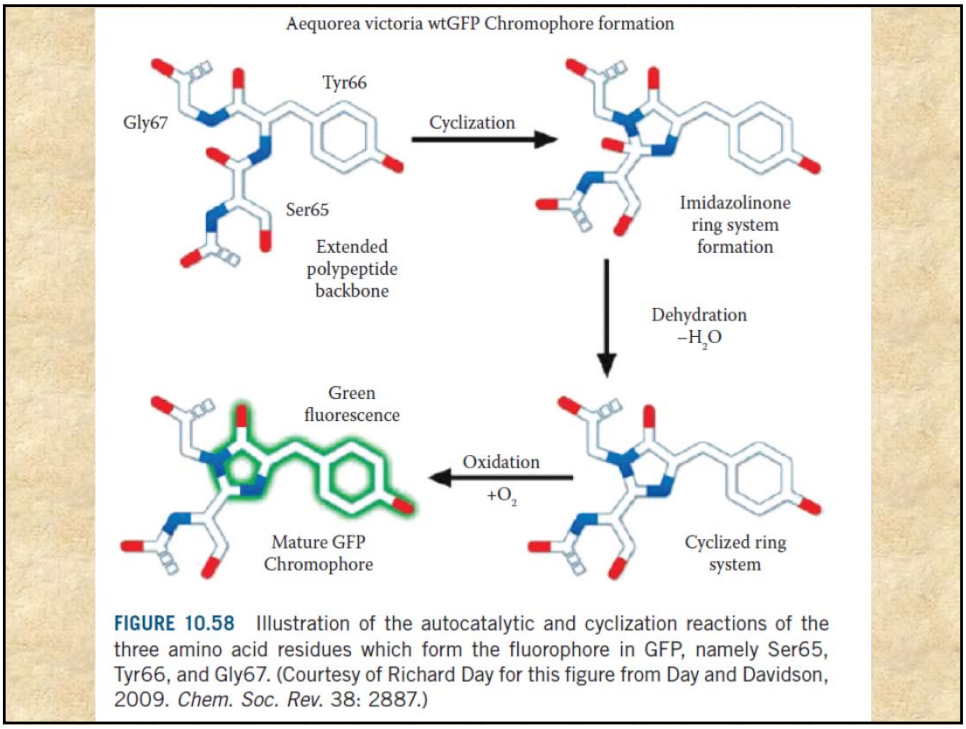

FIGURE 10.58 Illustration of the autocatalytic and cyclization reactions of the three amino acid residues which form the fluorophore in GFP, namely Ser65, Tyr66, and Gly67. (Courtesy of Richard Day for this figure from Day and Davidson, 2009. *Chem. Soc. Rev.* 38: 2887.)

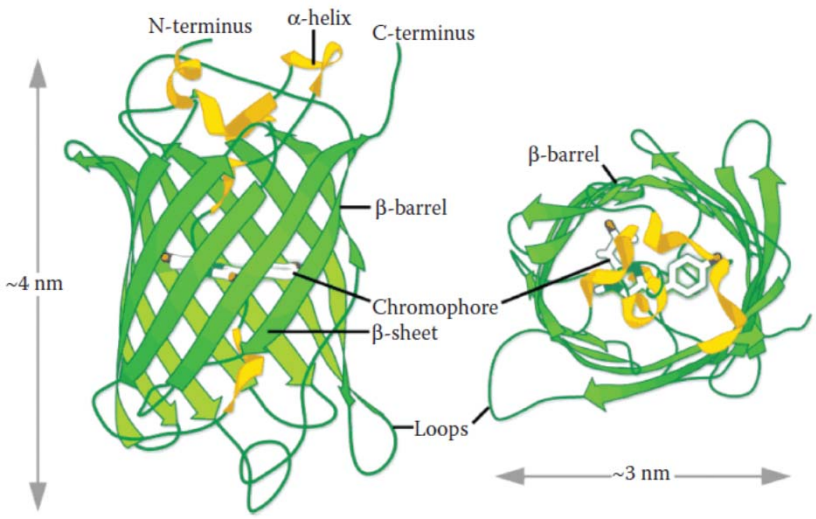

FIGURE 10.59 Illustration of the structure of GFP including the position of the chromophore in the protein structure. (Courtesy of Richard Day for this figure from Day and Davidson, 2009. *Chem. Soc. Rev.* 38: 2887.)

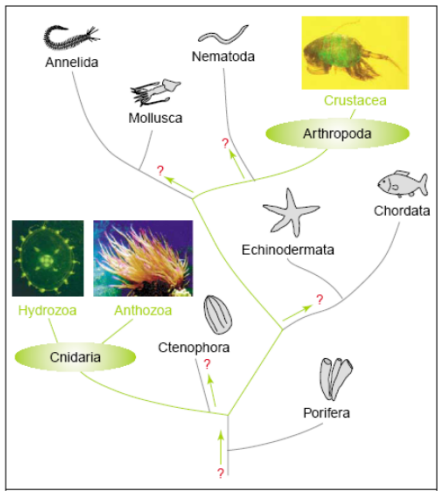

Figure 1. Positional relationship of the fluorescent protein-producing organisms on the phylogenetic tree. The phyla Cnidaria and Arthropoda (where GFP genes were found) and the branches connecting these phyla are highlighted in green. Photos show organisms representative of each phylum expressing GFP-like proteins: jellyfish *Phialidium* showing yellow fluorescence; sea anemone *Anemonia sulcata* with purple tentacle tips; and a copepod displaying green fluorescence. Question marks indicate possible, but unexplored, pathways of the evolution of FPs.

Fluorescent proteins as a toolkit for *in vivo* imaging

Dmitriy M. Chudakov, Sergey Lukyanov and Konstantin A. Lukyanov

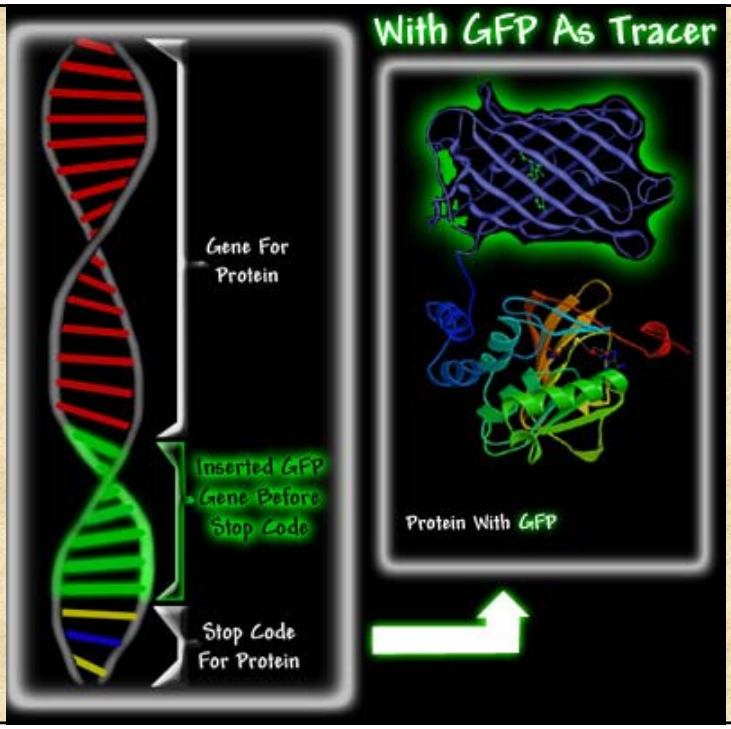

A number of new GFP proteins have been made using site directed mutagenesis to alter the amino acids near the chromophore and thus alter the absorption and fluorescence properties.

Proc. Natl. Acad. Sci. USA
Vol. 91, pp. 12501–12504, December 1994
Biochemistry

Wavelength mutations and posttranslational autoxidation of green fluorescent protein

(*Aequorea victoria*/blue fluorescent protein/*Escherichia coli*/imidazolidinone)

ROGER HEIM*, DOUGLAS C. PRASHER†, AND ROGER Y. TSIEN*‡

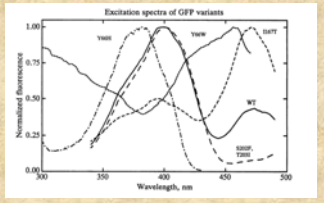

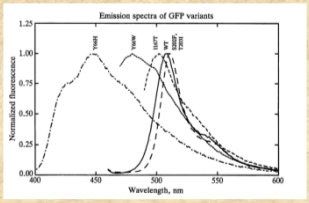

For all these reasons, it would be interesting to convert the *Aequorea* GFP excitation spectrum to a single peak, preferably at longer wavelengths. The cDNA was therefore subjected to random mutagenesis by hydroxylamine treatment or PCR. Approximately six thousand bacterial colonies on agar plates were illuminated with alternating 395- and 475-nm excitation and visually screened for altered excitation properties or emission colors. Although this number of colonies falls far short of saturating the possible mutations of a protein of 238 residues, interesting variants have already appeared.

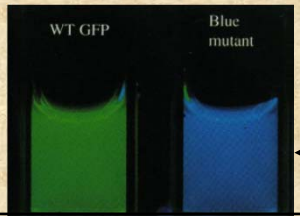

Tyr-66 replaced by His

Journal of Cell Science 120, 4247-4260

Advances in fluorescent protein technology

Nathan C. Shaner[1], George H. Patterson[2] and Michael W. Davidson[3]

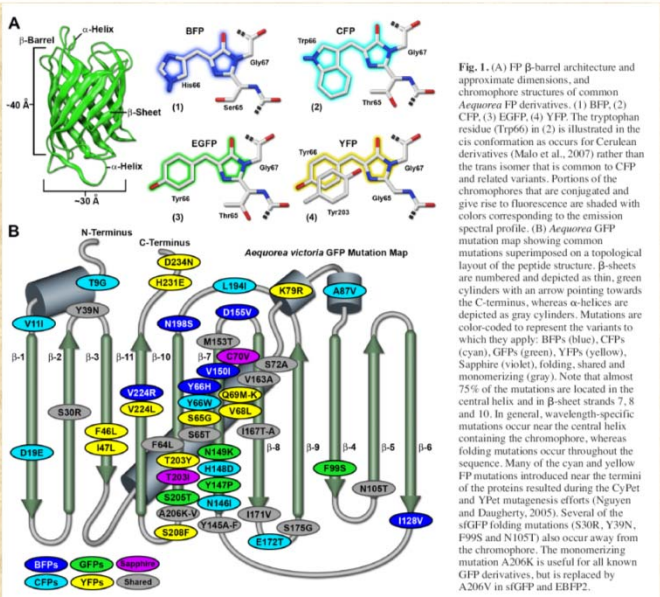

Fig. 1. (A) FP β-barrel architecture and approximate dimensions, and chromophore structures of common *Aequorea* FP derivatives. (1) BFP, (2) CFP, (3) EGFP, (4) YFP. The tryptophan residue (Trp66) in (2) is illustrated in the cis conformation as occurs for Cerulean derivatives (Malo et al., 2007) rather than the trans isomer that is common to CFP and related variants. Portions of the chromophores that are conjugated and give rise to fluorescence are shaded with colors corresponding to the emission spectral profile. (B) *Aequorea* GFP mutation map showing common mutations superimposed on a topological layout of the peptide structure. β-sheets are numbered and depicted as thin, green cylinders with an arrow pointing towards the C-terminus, whereas α-helices are depicted as gray cylinders. Mutations are color-coded to represent the variants to which they apply: BFPs (blue), CFPs (cyan), GFPs (green), YFPs (yellow), Sapphire (violet), folding, shared and monomerizing (gray). Note that almost 75% of the mutations are located in the central helix and in β-sheet strands 7, 8 and 10. In general, wavelength-specific mutations occur near the central helix containing the chromophore, whereas folding mutations occur throughout the sequence. Many of the cyan and yellow FP mutations introduced near the termini of the proteins resulted during the CyPet and YPet mutagenesis efforts (Nguyen and Daugherty, 2005). Several of the sfGFP folding mutations (S30R, Y39N, F99S and N105T) also occur away from the chromophore. The monomerizing mutation A206K is useful for all known GFP derivatives, but is replaced by A206V in sfGFP and EBFP2.

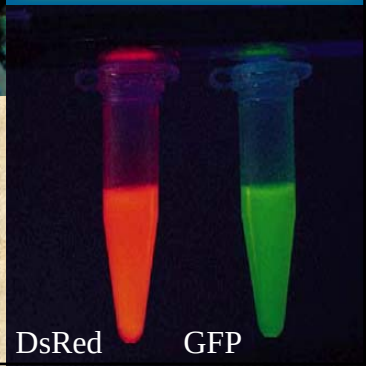

Another increasingly popular fluorescent protein is DsRed - originally isolated from the IndoPacific sea anemone relative *Discosoma* species

Journal of Cell Science 120, 4247-4260

Advances in fluorescent protein technology

Nathan C. Shaner[1], George H. Patterson[2] and Michael W. Davidson[3]

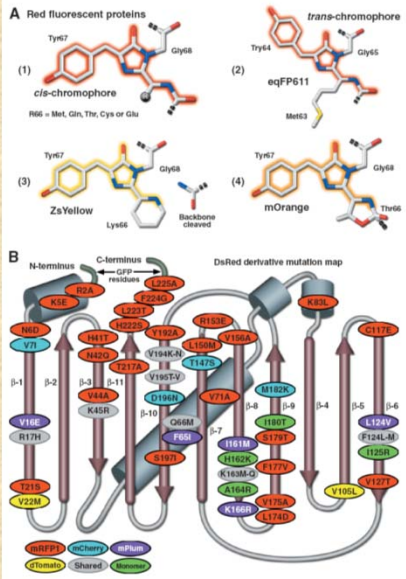

Fig. 2. (A) Chromophore structural variation in yellow, orange, and red FPs. (1) FPs derived from DsRed and other reef coral organisms thought to have a cis-chromophore. The residue at position 66 can be Met, Gln, Thr, Cys or Glu. (2) eqFP611, a red variant derived from *Entacmaea quadricolor*, is the only known FP featuring a trans-chromophore (Petersen et al., 2003). (3) ZsYellow (also zFP538), derived from the button polyp *Zoanthus*, features a novel three-ring chromophore that is created when the lysine residue at position 66 cyclizes with its own α-carbon to form a tetrahydropyridine ring conjugated to the chromophore (Remington et al., 2005). (4) mOrange, one of the mFruit proteins (Shaner et al., 2004), also features a three-ring chromophore where Thr66 cyclizes with the preceding carbonyl carbon to yield a partially conjugated oxazole ring (Shu et al., 2006). (B) DsRed mutation map showing mutations of useful variants superimposed on a topological layout of the peptide structure. β-sheets are numbered and depicted as thin, red cylinders with an arrow pointing towards the C-terminus, whereas α-helices are depicted by gray cylinders. Extensions of the N- and C-termini due to the addition of amino acids derived from GFP to improve fusion performance are shaded in light green. Mutations are color-coded to represent the variants to which they apply: mRFP1 (red), mCherry (cyan), mPlum (violet), dTomato (yellow), monomerizing mutations (green) and shared mutations (gray). Note that unlike the cluster of mutations surrounding the chromophore for *Aequorea* GFP variants (Fig. 1), red FP mutations are distributed throughout the sequence.

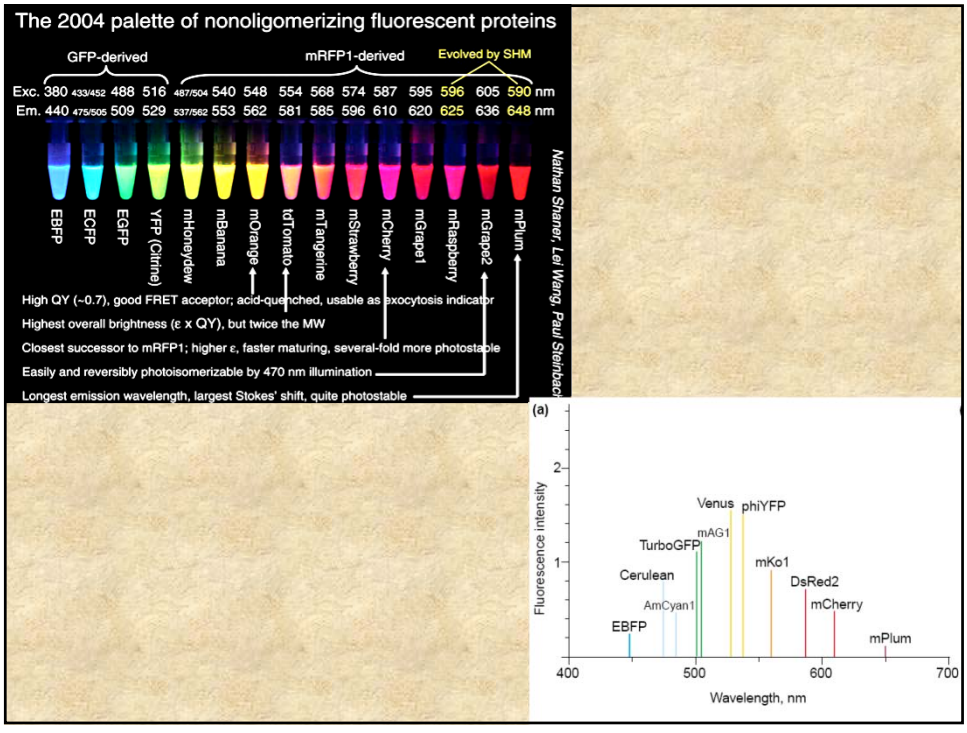

NATURE METHODS | VOL.2 NO.12 | DECEMBER 2005 | 905

A guide to choosing fluorescent proteins

Nathan C Shaner[1,2], Paul A Steinbach[1,3] & Roger Y Tsien[1,3,4]

The recent explosion in the diversity of available fluorescent proteins (FPs)[1–16] promises a wide variety of new tools for biological imaging. With no unified standard for assessing these tools, however, a researcher is faced with difficult questions. Which FPs are best for general use? Which are the brightest? What additional factors determine which are best for a given experiment? Although in many cases, a trial-and-error approach may still be necessary in determining the answers to these questions, a unified characterization of the best available FPs provides a useful guide in narrowing down the options.

'Brightness' and expression **Photostability** **Environmental sensitivity**

Oligomerization and toxicity **Multiple labeling**

BOX 1 RECOMMENDATIONS BY SPECTRAL CLASS

Far-red. mPlum is the only reasonably bright and photostable far-red monomer available. Although it is not as bright as many shorter-wavelength options, it should be used when spectral separation from other FPs is critical, and it may give some advantage when imaging thicker tissues. AQ143, a mutated anemone chromoprotein, has comparable brightness (ε = 90 (mM • cm)$^{-1}$, quantum yield (QY) = 0.04) and even longer wavelengths (excitation, 595 nm; emission, 655 nm), but it is still tetrameric[31].

Red. mCherry is the best general-purpose red monomer owing to its superior photostability. Its predecessor mRFP1 is now obsolete. The tandem dimer tdTomato is equally photostable but twice the molecular weight of mCherry, and may be used when fusion tag size does not interfere with protein function. mStrawberry is the brightest red monomer, but it is less photostable than mCherry, and should be avoided when photostability is critical. We do not recommend using J-Red and DsRed-Monomer.

Orange. mOrange is the brightest orange monomer, but should not be used when photostability is critical or when it is targeted to regions of low or unstable pH. mKO is extremely photostable and should be used for long-term or intensive imaging experiments or when targeting to an acidic or pH-unstable environment.

Yellow-green. The widely used variant EYFP is obsolete and inferior to mCitrine, Venus and YPet. Each of these should perform well in most applications. YPet should be used in conjunction with the CFP variant CyPet for FRET applications.

Green. Although it has a more pronounced fast bleaching component than the common variant EGFP, the newer variant Emerald exhibits far more efficient folding at 37 °C and will generally perform much better than EGFP.

Cyan. Cerulean is the brightest CFP variant and folds most efficiently at 37 °C, and thus, it is probably the best general-purpose CFP. Its photostability under arc-lamp illumination, however, is much lower than that of other CFP variants. CyPet appears superior to mCFP in that it has a somewhat more blue-shifted and narrower emission peak, and displays efficient FRET with YFP variant YPet, but it expresses relatively poorly at 37 °C.

UV-excitable green. T-Sapphire is potentially useful as a FRET donor to orange or red monomers.

Table 1 | Properties of the best FP variants[a,b]

Class	Protein	Source laboratory (references)	Excitation[c] (nm)	Emission[d] (nm)	Brightness[e]	Photostability[f]	pKa	Oligomerization
Far-red	mPlum[g]	Tsien (5)	590	649	4.1	53	<4.5	Monomer
Red	mCherry[g]	Tsien (4)	587	610	16	96	<4.5	Monomer
	tdTomato[g]	Tsien (4)	554	581	95	98	4.7	Tandem dimer
	mStrawberry[g]	Tsien (4)	574	596	26	15	<4.5	Monomer
	J-Red[h]	Evrogen	584	610	8.8*	13	5.0	Dimer
	DsRed-monomer[h]	Clontech	556	586	3.5	16	4.5	Monomer
Orange	mOrange[g]	Tsien (4)	548	562	49	9.0	6.5	Monomer
	mKO	MBL Intl. (10)	548	559	31*	122	5.0	Monomer
Yellow-green	mCitrine[i]	Tsien (16,23)	516	529	59	49	5.7	Monomer
	Venus	Miyawaki (1)	515	528	53*	15	6.0	Weak dimer[i]
	YPet[g]	Daugherty (2)	517	530	80*	49	5.6	Weak dimer[i]
	EYFP	Invitrogen (18)	514	527	51	60	6.9	Weak dimer[i]
Green	Emerald[g]	Invitrogen (18)	487	509	39	0.69[k]	6.0	Weak dimer[i]
	EGFP	Clontech[i]	488	507	34	174	6.0	Weak dimer[i]
Cyan	CyPet	Daugherty (2)	435	477	18*	59	5.0	Weak dimer[i]
	mCFPm[m]	Tsien (23)	433	475	13	64	4.7	Monomer
	Cerulean[g]	Piston (3)	433	475	27*	36	4.7	Weak dimer[i]
UV-excitable green	T-Sapphire[g]	Griesbeck (6)	399	511	26*	25	4.9	Weak dimer[i]

http://nic.ucsf.edu/FPvisualization/

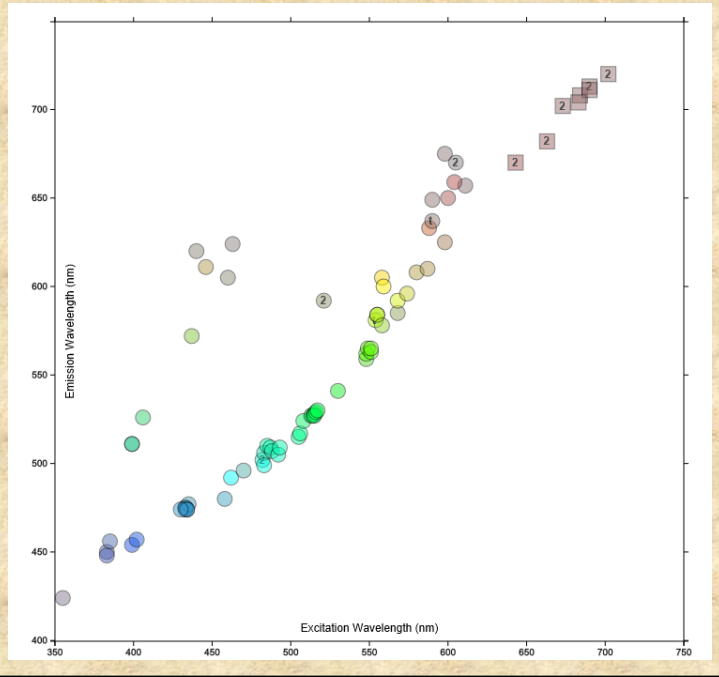

http://nic.ucsf.edu/FPvisualization/

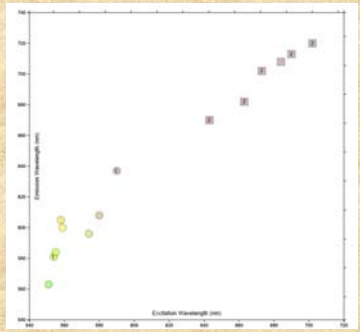

Select excitation wavelength above 524nm
And extinction coefficient above 89,000

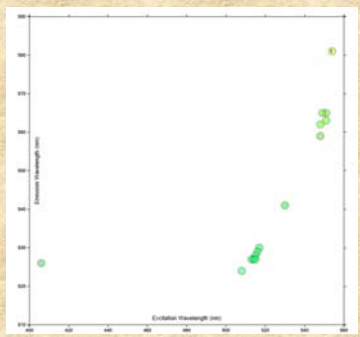

Select emission wavelength above 520nm
And quantum yield above 0.5

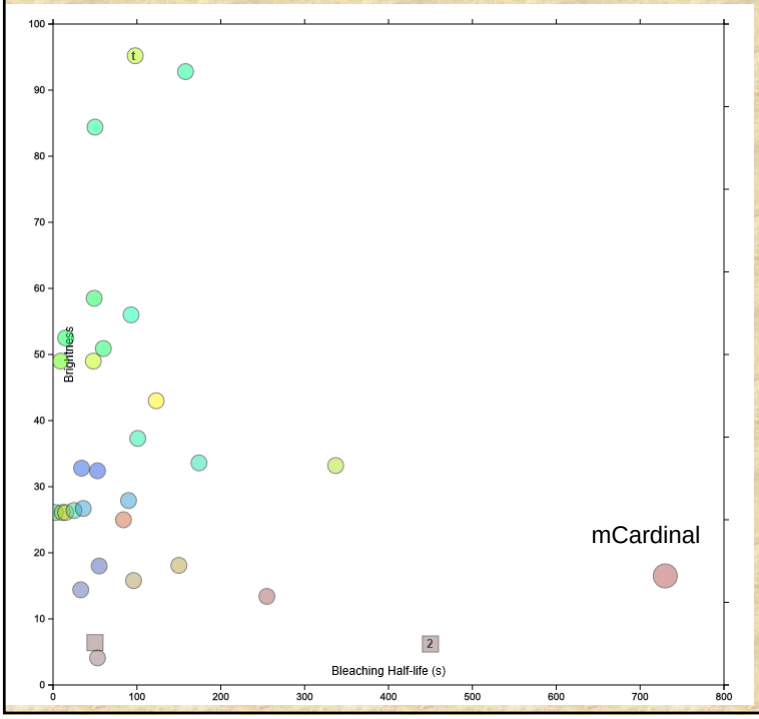

Plot different scales:

Brightness vs Stability (bleaching half-life)

Move cursor to identify protein

FlAsH-EDT2 labeling (FlAsH tag)

Specific Covalent Labeling of Recombinant Protein Molecules Inside Live Cells

B. Albert Griffin,* Stephen R. Adams, Roger Y. Tsien†

SCIENCE VOL 281 10 JULY 1998

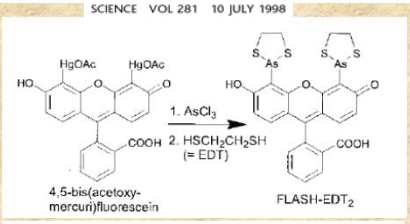

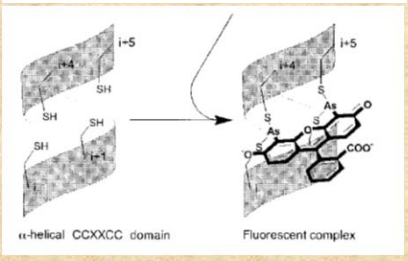

The original motif "CCXXCC" often gave rise to significant nonspecific background.

The use of the "CCPGCC" motif led to reduced background

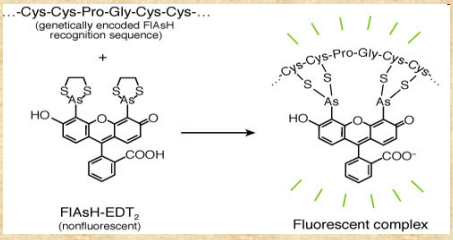

New motifs include "HRWCCPGCCKTF" and "FLNCCPGCCMEP"

ReAsh

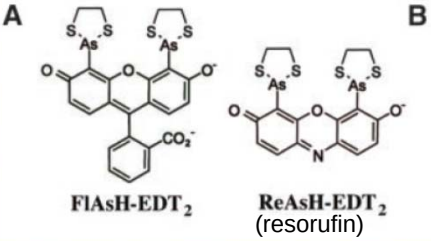

Multicolor and Electron Microscopic Imaging of Connexin Trafficking

Guido Gaietta,[1] Thomas J. Deerinck,[1] Stephen R. Adams,[2] James Bouwer,[1] Oded Tour,[2*] Dale W. Laird,[3] Gina E. Sosinsky,[1] Roger Y. Tsien,[2*] Mark H. Ellisman[1†]

SCIENCE VOL 296 19 APRIL 2002

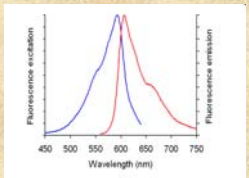

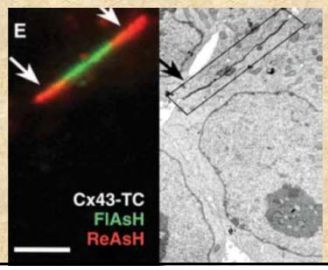

Tetracysteines on connexin43 were pulse-labeled with FlAsH (green) and subsequently ReAsH (red), thus distinguishing old from new connexins, respectively. ReAsH is also visualized in EM using photooxidation (E) (right).

Bimolecular Fluorescence Complementation (BiFC)

Nat Biotechnol. 2003 May ; 21(5): 539–545.

Simultaneous visualization of multiple protein interactions in living cells using multicolor fluorescence complementation analysis

Chang-Deng Hu and **Tom K. Kerppola***

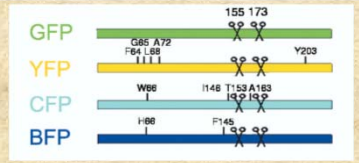

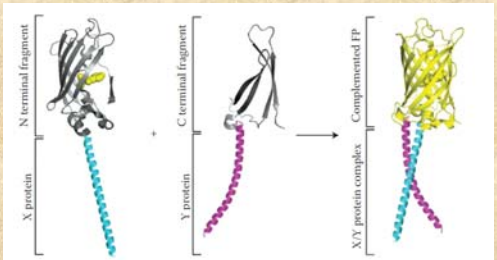

FIGURE 10.62 Illustration of the biomolecular fluorescence complementation method. (From Kodama and Hu (2012) *Biotechniques* 53: 285.)

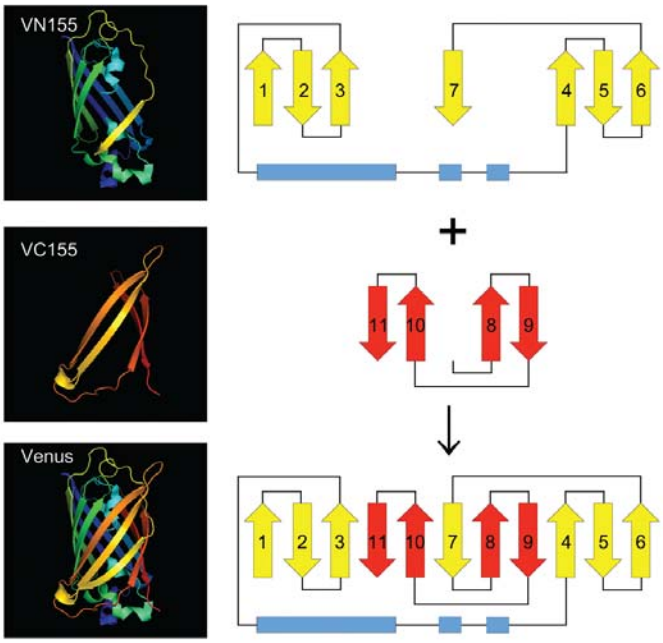

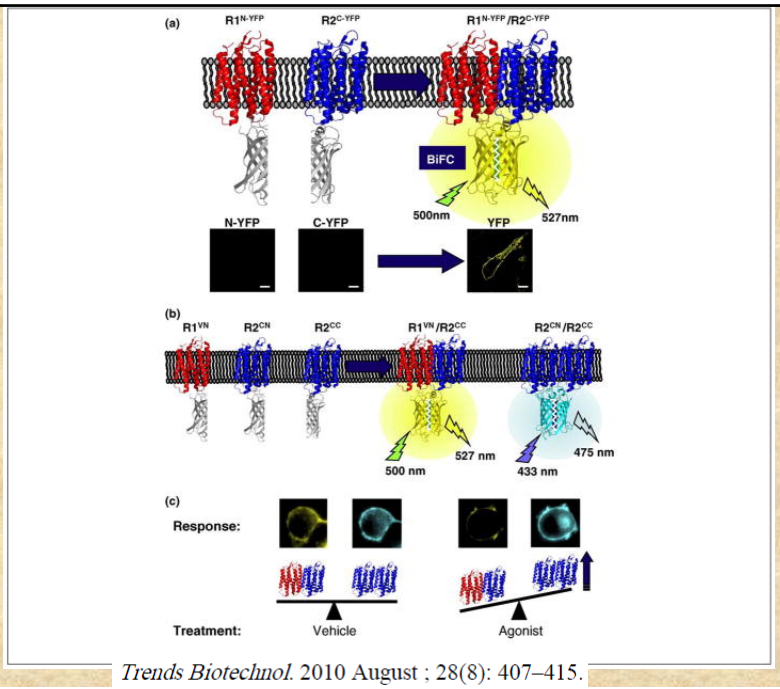

Trends Biotechnol. 2010 August ; 28(8): 407–415.

Francisco Ciruela[1], **Jean-Pierre Vilardaga**[2,3], and **Víctor Fernández-Dueñas**[1]

HALO tags

Fluorescence Fluctuation Spectroscopy Approaches to the Study of Receptors in Live Cells

David M. Jameson[*,1], Nicholas G. James[*], Joseph P. Albanesi[†]

Methods in Enzymology, Volume 519

2013

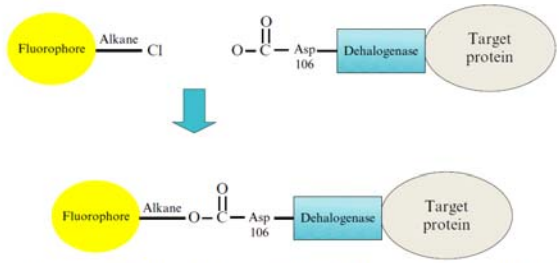

Figure 3.7 Schematic illustrating the principle underlying the HaloTag method. A fluorescent probe is linked to a haloalkane, and the bacterial dehalogenase enzyme is recombinantly fused to the target protein. The fluorescent haloalkane can form a stable covalent linkage with the dehalogenase.

SNAP tags

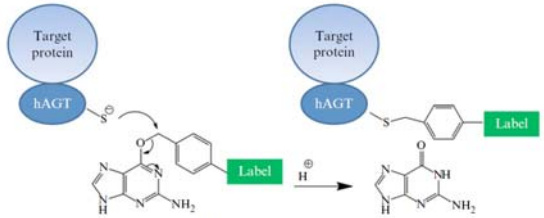

Figure 3.8 Mechanism of covalent labeling of hAGT, which is fused to a target protein, with a fluorescent label linked onto an O^6-benzylguanine derivative. *Figure modified from Keppler et al. (2003).*

Demonstrating FRET by photobleaching acceptor

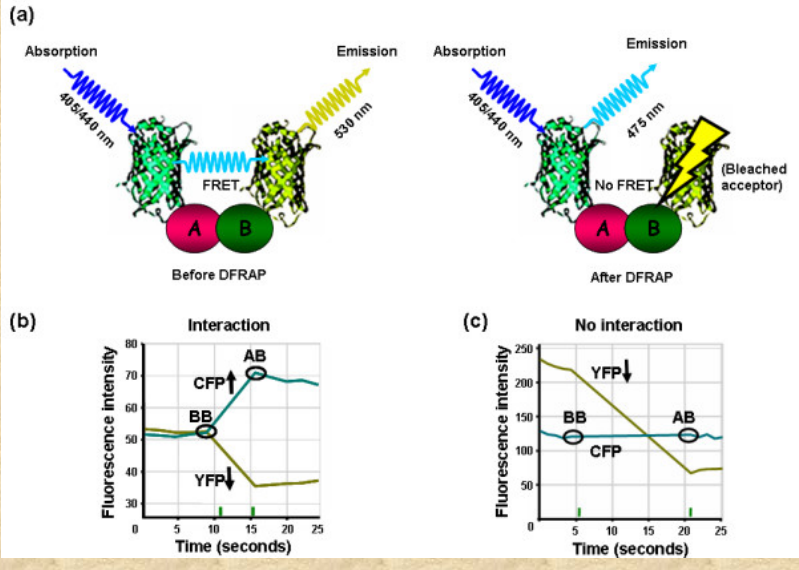

http://paxomuse.tumblr.com/photobleaching-model

Molecular Vision 2008; 14:1282-1287 <http://www.molvis.org/molvis/v14/a152>
Received 12 May 2008 | Accepted 2 July 2008 | Published 10 July 2008

Protein-protein interactions between lens vimentin and αB-crystallin using FRET acceptor photobleaching

Shuhua Song, Mark J. Hanson, Bing-Fen Liu, Leo T. Chylack Jr., Jack J-N. Liang

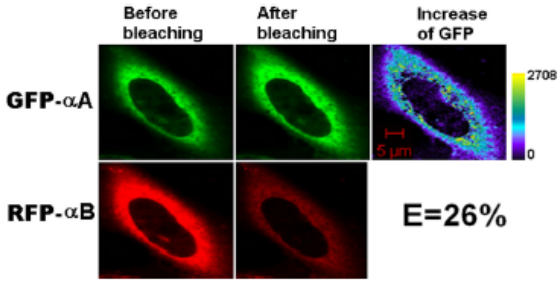

Figure 2. Representative laser scanning microscopy images of HeLa cells co-transfected with the positive controls, GFP-αA and RFP-αB. The constructs were co-transfected into HeLa cells. After culture, laser scanning microscopy (LSM) images were taken. αA- and αB-crystallins are known to have a strong subunit-subunit interaction. The energy transfer efficiency is high. The increase of GFP fluorescence intensity is converted to pseudocolor (right panel) that displays variations of pixel gray scales with color.